Journal of Constructional Steel Research 210 (2023) 108096

Contents lists available at ScienceDirect

Journal of Constructional Steel Research

journal homepage: www.elsevier.com/locate/jcsr

Optimal design method of the load-level isolation system for industrial steel racking

Enrico Bernardi [a,b], Marco Donà [b,a,*], Ping Tan [c,a], Francesca da Porto [b]

[a] Earthquake Engineering Research & Test Center, Guangzhou University, 510006 Guangzhou, China
[b] Department of Geosciences, University of Padova, 35131 Padova, Italy
[c] School of Civil Engineering, Guangzhou University, 510006 Guangzhou, China

ARTICLE INFO

Keywords:
Industrial steel racking
Standard pallet racks
Load-level isolation system
Tuned mass damper
Structural optimization
Tuning of the isolation system

ABSTRACT

This paper focuses on an innovative system for mitigating seismic actions on industrial steel racking, called Load-Level Isolation System (LLIS). It consists of placing isolators directly between the pallet masses and the load level, thus exploiting the pallet masses (much greater than the structural mass) as tuned mass dampers. Specifically, the paper aims to derive a general design procedure for the LLIS, based on the amount of mass isolated, the position of the LLIS within the rack, and the main dynamic characteristics of the structural system. To this end, an analytical optimization method is proposed, based on the minimization of the displacement variance of a reduced structural model, representative of the rack dynamics with the LLIS. This method is applied parametrically to derive the optimal damping and frequency values of the LLIS in various design situations, and a sensitivity analysis is subsequently conducted to propose cost-effective LLIS design solutions. Prediction models of the LLIS parameters are therefore provided, as well as a simple step-by-step procedure for designing the control system. Finally, a case study is presented, with the dual objectives of showing the application of the design procedure and the effectiveness of the LLIS in mitigating seismic effects in a standard pallet rack. The results of the Time-History analysis demonstrate the validity of the proposed design method and the possibility of achieving large reductions in the seismic response of the rack using this control system, and up to 60% for both maximum displacements and axial forces of the uprights.

Table of notation

A	Cross section area of the structural elements
a_{MAX}	Maximum pallet accelerations
BI	Base isolation
$\boldsymbol{C}$	Damping matrix of the equivalent 3-DOF system
$\boldsymbol{C}'$	Dimensionless damping matrix of the equivalent 3-DOF system
c_i	Structural damping constants
c_{IS}	Damping constant of the isolation system
c_L (c_U)	Damping constant of the lower (upper) DOF of the equivalent 3-DOF system
d_{IS}	Maximum isolation drift
d_{MAX}	Maximum displacement at the rack top
E	Elastic modulus of steel
$\mathbf{G}(\rho)$	Dimensionless displacement FRF
Gi	Components of the vector $\mathbf{G}(\rho)$
h_L (h_U)	Total height of the racking part below (above) the LLIS
J_d	Optimization problem / optimal solution
J_d', J_d''	Optimal cost-effective solutions (requiring less damping than J_d)
J_i	Moment of inertia with respect to the i-axes
$\boldsymbol{K}$	Stiffness matrix of the equivalent 3-DOF system
$\boldsymbol{K}'$	Dimensionless stiffness matrix of the equivalent 3-DOF system
k_{IS}	Stiffness constant of the isolation system
k_L (k_U)	Stiffness constant of the lower (upper) DOF of the equivalent 3-DOF system
$k_{\varphi,Y}$	Rotational stiffness around Y-axis of the beam-to-column connections
k_{φ,Y_base}	Rotational stiffness around Y-axis of the base connections
LL	Load-Level
LLIS	Load-Level Isolation System
$\boldsymbol{M}$	Mass matrix of the equivalent 3-DOF system
$\boldsymbol{M}'$	Dimensionless mass matrix of the equivalent 3-DOF system

* Corresponding author at: Department of Geosciences, University of Padova, 35131 Padova, Italy.
E-mail address: marco.dona.1@unipd.it (M. Donà).

https://doi.org/10.1016/j.jcsr.2023.108096
Received 15 March 2023; Received in revised form 21 June 2023; Accepted 24 June 2023
Available online 30 June 2023

m_{IS}	Mass constant of the isolation system (isolated mass)
m_L (m_U)	Mass constant of the lower (upper) DOF of the equivalent 3-DOF system
$\boldsymbol{M_L}$ ($\boldsymbol{M_U}$)	Mass matrix of the structural part below (above) the LLIS
OF_d	Objective function: minimization of m_U displacement variance
$OF_{d,norm}$	Normalized objective function
PSD	Power Spectral Density
R^2	Coefficient of determination
$RMSE$	Root Mean Square Error
$\mathbf{S}(\omega)$	PSD function of a zero-mean Gaussian stochastic process
S_0	PSD function of a white noise zero-mean Gaussian stochastic process
S_a	Spectral acceleration
SSE	Sum Squared Error (sum of squared estimate of errors)
μ_{IS}	Isolation mass ratio ($=m_{IS}/m_L$)
μ_U	Superstructure mass ratio ($=m_U/m_L$)
ν_{IS}	Isolation frequency ratio ($=\omega_{IS}/\omega_L$)
$\nu_{IS,opt}$	Optimal isolation frequency ratio
ν_U	Superstructure frequency ratio ($=\omega_U/\omega_L$)
ξ_{IS}	Isolation damping ratio
$\xi_{IS,opt}$	Optimal isolation damping ratio
ξ_L (ξ_U)	Structural damping ratio of the lower (upper) DOF of the equivalent 3-DOF system
ρ	Normalized seismic input angular frequency ($=\omega/\omega_L$)
$\boldsymbol{\sigma}_d^2$	Vector of the displacement response variance of the equivalent 3-DOF system
$\sigma_{d,3}^2$	Variance of m_U displacement
$\sigma_{d,IS}^2$	Variance of isolation drift
σ_{IS}'	Normalized variance of isolation drift
$\boldsymbol{\tau}$	unit rigid displacement vector [1,1,1]
$\phi_{1,L}$ ($\phi_{1,U}$)	First-mode eigenvector of the structural part below (above) the LLIS
ω	Seismic input angular frequency
ω_{IS}	Angular frequency of the isolation system
ω_L (ω_U)	Angular frequency of the lower (upper) DOF of the equivalent 3-DOF system

1. Introduction

Industrial steel racks are becoming increasingly popular due to the rise of e-commerce and the logistics sector. Various storage systems are currently available (EN15878 CEN [1], EN15512 CEN [2], Shaheen and Rasmussen [3]), such as the standard pallet racking systems, the drive-in and drive-through racks, and the flow-through racks.

All these storage systems are characterized by being composed of cold-formed open-section steel profiles, and by having a very low self-weight to total payload ratio, equal to about 5% (Bernuzzi and Simoncelli [4]). Furthermore, the structural behavior is very different in the two main directions. In the cross-aisle (transverse) direction, the structural configuration is fairly rigid, and consists of trusses composed of uprights and diagonal/transverse bracing elements; whereas, in the down-aisle (longitudinal) direction, the rack is generally very flexible, with moment-resistant frames consisting of uprights and pallet beams, connected to each other by means of semi-rigid joints (EN1993-1-8 CEN [5]).

Several research works are currently available on the structural and seismic performance of storage systems. Some of these investigated the behavior of specific rack components, such as the non-linear behavior of beam-to-column and base connections, both experimental (e.g., Bernuzzi and Castiglioni [6], Yin et al. [7], Dai et al. [8], [9], Gusella et al. [10], Zhao et al. [11], Baldassino and Zandonini [12], Petrone et al. [13]) and numerical (e.g., Jovanović et al. [14], Gabbianelli et al. [15], Huang et al. [16]), and the axial and flexural hysteretic behavior of open-section steel profiles, including instability effects (Padilla-Llano et al. [17,18]). Other studies concerned the seismic vulnerability assessment of entire storage systems, both through non-linear numerical analyzes (e.g., Yin et al. [19,20]) and experimental tests on shaking table (e.g., Jacobsen and Tremblay [21]). Various investigations, including pushover tests of real racks, component tests and numerical simulations were then carried out within two important experimental campaigns, SEISRACKS (Proença et al. [22]) and SEISRACKS2 (Drei et al. [23]). The latter significantly supported the definition of the current seismic standard EN16681 (CEN [24]).

Overall, the previous studies highlighted the great seismic vulnerability of these storage systems. This was also confirmed by the recent studies by Gabbianelli et al. [15] and Piredda et al. [25] on the seismic fragility of pallet racking, which showed that the collapse of these structural systems can occur for very low values of spectral acceleration (S_a). In addition, another critical aspect is the possible triggering of pallet sliding due to high accelerations on pallet masses.

Although some researchers proved that pallet sliding can be beneficial, as it can reduce seismic forces (e.g., Jacobsen and Tremblay [21], Castiglioni et al. [26]), this phenomenon is not controlled, and can cause the goods to fall (especially from higher load levels) in the case of strong seismic events, posing a serious risk to the safety of workers. It should also be considered that damage to both racking and stored goods (due to their possible fall) contribute significantly to the expected seismic losses of production activities, both direct and indirect due to business interruption (e.g., Brown et al. [27], Donà et al. [28]).

For all these reasons, various technological solutions were proposed in recent years to improve the overall seismic performance of these structures, which concern the base seismic isolation (e.g., Filiatrault et al. [29], Franco et al. [30]) and the application of special dissipative systems (e.g., Shaheen and Rasmussen [31]). To date, more than a few rack-specific isolation systems were proposed, most of which are described in the literature review by Simoncelli et al. [32].

These devices differ from the conventional ones used in civil structures due to the peculiarities of racking, such as: the magnitude of the vertical loads involved, much less than in civil structures; the high uncertainty about the arrangement of inertial masses (or pallets) in operating conditions, which requires treating the mass distribution as a design variable; the specific geometries and dynamic performances of these structural systems, very different in the two main directions. Due to the generally high vibration periods of the racks in the down-aisle direction, most of these isolation systems operate in the cross-aisle direction only, thus also reducing interference with goods handling operations (Simoncelli et al. [32]). Nonetheless, some researchers also proposed bidirectional isolation devices, such as the one proposed by Ferrari et al. [33,34].

Although these new seismic mitigation technologies for industrial racks are receiving increasing attention, their spread is limited by various factors. In particular, the first of these is the cost of the devices, which should be very low, given the very low costs of racking systems compared to building structures. In addition, there are no specific standards or guidelines for the design and installation of these rack-mounted devices, which allow considering the peculiarities of these structural systems as described above (e.g., the high mass distribution uncertainty).

Another innovative seismic mitigation solution for racking systems, recently analyzed for a case study pallet rack by Donà et al. [35], consists of using isolation devices between pallet units and load levels. This technique, called Load-Level Isolation System (LLIS), aims to use the stored mass (prevailing over the structural mass) as a Tuned Mass Damper (TMD) to reduce the structural seismic response. The LLIS, which can be applied to one or more load levels, has some advantages over base isolation (BI). These include the fact that space restrictions at the base of the rack, to ensure the design displacement of the isolators, are no longer necessary; moreover, the design of the LLIS compared to that of the BI is less affected by the variable distribution of the masses as well as by possible lifting issues; lastly, the LLIS allows greater ease of installation, especially in existing rack systems, where this technique

would be an effective retrofit solution and a viable alternative to traditional solutions, such as inserting bracing or strengthening uprights (which leads to increased seismic accelerations), or limiting the maximum allowable payload (using the rack only partially).

In fact, the LLIS can be anchored to the existing pallet beams, creating a sliding plane on the extrados of these beams by means of a second level of equivalent pallet beams. Possible isolation/dissipation technological solutions, not addressed in this paper, should be such as to avoid substantial changes to the racking layout, and such as not to significantly increase the maximum vertical load on the uprights. Conventional rolling or sliding bearings (of limited height and weight) could be used for this purpose, along with recentering and dissipative devices placed between the two levels of beams (taking advantage of the extra height given by the second level of beams). Clearly, when the LLIS is placed on top of the rack, its size is no longer a significant issue.

The LLIS analyzed in the previous study (Donà et al. [35]), in various installation configurations, was found to be very effective in reducing seismic stresses on uprights and accelerations on pallets for the case study rack. However, its general application to various storage systems requires a specific method for optimizing the isolation parameters (i.e., isolation frequency and isolation damping ratio). In this context, this paper aims to provide a general LLIS design methodology, which allows taking into account, as design variables, the dynamic characteristics of the racking, the amount of isolated mass, and its position inside the racking.

After defining the simplified structural model that represents the dynamics of the rack equipped with the LLIS, the paper presents an analytical method for optimizing the isolation parameters based on minimizing the overall displacement variance of the rack. The optimization results are then exploited for a sensitivity analysis to derive more cost-effective solutions for the LLIS. Then, based on these solutions, prediction models of the LLIS parameters are provided, and a specific design procedure of this control system is proposed. Finally, a case study is presented, with the dual aim of showing the application of the design procedure and the effectiveness of the LLIS in mitigating seismic effects in a standard pallet racking. Specifically, a representative single-entry rack with five spans and eight load levels is selected and analyzed in Time-History (TH), under a set of bi-directional and spectrum-compatible natural events, in the case with and without LLIS.

2. Equivalent dynamic model of racks

For the LLIS optimization study, the dynamics of the pallet racking can be investigated through the simplified three degrees-of-freedom (DOFs) system represented in Fig. 1. In particular, the isolated load levels (where the LLIS is installed) can be modeled by a single degree-of-freedom (SDOF) system, assuming the total isolated mass as the equivalent mass m_{IS}, and the specific stiffness (k_{IS}) and damping (c_{IS}) coefficients of the isolation system. Then, the structural part without LLIS can be modeled by a 2-DOF system, where the lower DOF (denoted by subscript $_L$) represents the part of the rack below the isolation system, and the upper DOF (denoted by subscript $_U$) represents the remaining part of the rack, which includes the isolated load levels, but without the associated pallet masses, and the upper load levels. Therefore, the LLIS and the upper DOF (upper part of the rack) are both connected to the lower DOF (lower part of the rack), as shown in Fig. 1.

The parameters m_L, k_L and c_L are the modal mass, stiffness and damping coefficients of the lower DOF, respectively, whereas m_U, k_U and c_U are the same parameters for the upper DOF. These parameters refer to the main vibration mode of the two independent racking parts, separated by the LLIS. Generally, this vibration mode is the first one in the cross-aisle direction, as the LLIS is primarily devised to operate in the transverse direction only (like most base isolation devices, as stated above). The main reasons for this are the relatively high vibration periods of the racks in the down-aisle direction, and the need to avoid possible collisions of the pallet on the uprights (in the same direction). Therefore, the parameters of the equivalent model can be calculated as follows:

$$\begin{aligned} m_L &= \phi_{1,L}^T M_L \phi_{1,L}, m_U = \phi_{1,U}^T M_U \phi_{1,U} \\ c_L &= 2\xi_L \omega_L m_L \ , \ c_U = 2\xi_U \omega_U m_U \\ k_L &= \omega_L^2 m_L \ , \ k_U = \omega_U^2 m_U \end{aligned} \tag{1}$$

$\boldsymbol{M_L}$ and $\boldsymbol{M_U}$ are the mass matrices of the racking parts respectively below and above the LLIS; $\phi_{1,L}$ and $\phi_{1,U}$ are the related eigenvectors of the reference mode (both normalized to one), and ξ_L, ξ_U and ω_L, ω_U are the associated equivalent damping ratios and angular frequencies.

For the sake of completeness, the definition of c_{IS} and k_{IS} as a function of the angular frequency (ω_{IS}) and the equivalent damping ratio (ξ_{IS}) of the isolation system is also given below:

$$\begin{aligned} c_{IS} &= 2\xi_{IS}\omega_{IS} m_{IS} \\ k_{IS} &= \omega_{IS}^2 m_{IS} \end{aligned} \tag{2}$$

The mass ($\boldsymbol{M}$), damping ($\boldsymbol{C}$) and stiffness ($\boldsymbol{K}$) matrices of the equivalent 3-DOF system are therefore:

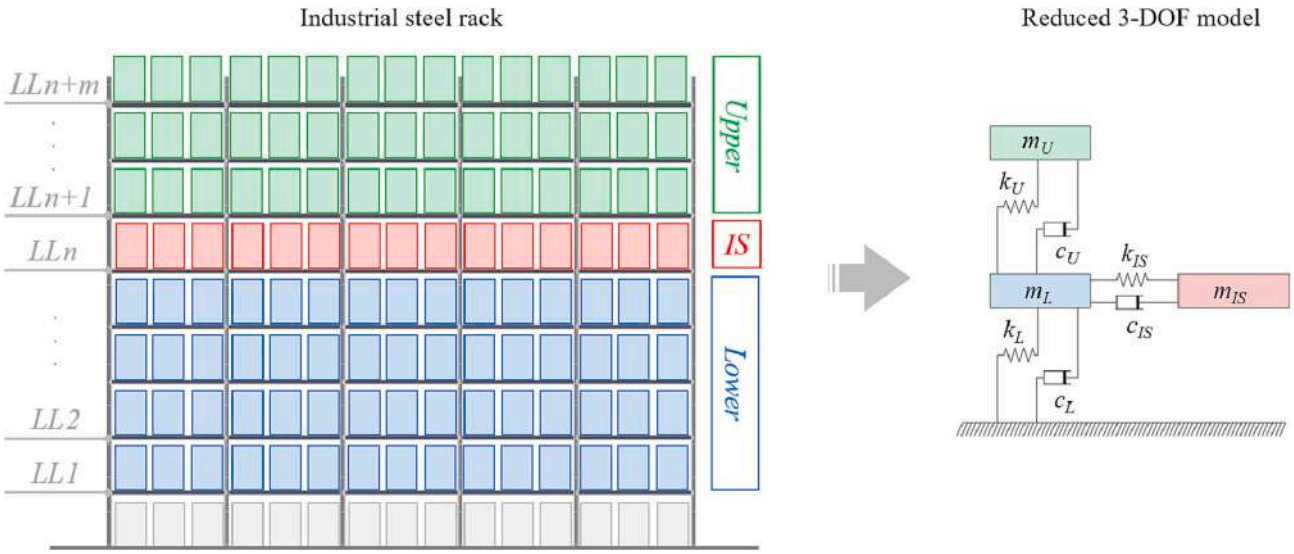

Fig. 1. Equivalent 3-DOF system of the rack controlled by the LLIS.

$$M = \begin{bmatrix} m_L & 0 & 0 \\ 0 & m_{IS} & 0 \\ 0 & 0 & m_U \end{bmatrix}$$

$$C = \begin{bmatrix} c_L + c_{IS} + c_U & -c_{IS} & -c_U \\ -c_{IS} & c_{IS} & 0 \\ -c_U & 0 & c_U \end{bmatrix} \quad (3)$$

$$K = \begin{bmatrix} k_L + k_{IS} + k_U & -k_{IS} & -k_U \\ -k_{IS} & k_{IS} & 0 \\ -k_U & 0 & k_U \end{bmatrix}$$

To generalize the optimization study, the parameters of the equivalent 3-DOF system can be normalized to the characteristics of the DOF representing the lower part of the rack, thus defining the following dimensionless ratios of mass (μ_{IS} and μ_U) and angular frequency (ν_{IS} and ν_U):

$$\mu_{IS} = \frac{m_{IS}}{m_L} \quad , \quad \mu_U = \frac{m_U}{m_L}$$
$$\nu_{IS} = \frac{\omega_{IS}}{\omega_L} \quad , \quad \nu_U = \frac{\omega_U}{\omega_L} \quad (4)$$

Through these dimensionless ratios, the previous matrices of the 3-DOF system can also be expressed in dimensionless form ($\boldsymbol{M}^{/}$, $\boldsymbol{C}^{/}$ and $\boldsymbol{K}^{/}$), namely:

$$M^{/} = \begin{bmatrix} 1 & 0 & 0 \\ 0 & \mu_{IS} & 0 \\ 0 & 0 & \mu_U \end{bmatrix}$$

$$C^{/} = \begin{bmatrix} 2\xi_L + 2\xi_{IS}\nu_{IS}\mu_{IS} + 2\xi_U\nu_U\mu_U & -2\xi_{IS}\nu_{IS}\mu_{IS} & -2\xi_U\nu_U\mu_U \\ -2\xi_{IS}\nu_{IS}\mu_{IS} & 2\xi_{IS}\nu_{IS}\mu_{IS} & 0 \\ -2\xi_U\nu_U\mu_U & 0 & 2\xi_U\nu_U\mu_U \end{bmatrix} \quad (5)$$

$$K^{/} = \begin{bmatrix} 1 + {\nu_{IS}}^2\mu_{IS} + {\nu_U}^2\mu_U & -{\nu_{IS}}^2\mu_{IS} & -{\nu_U}^2\mu_U \\ -{\nu_{IS}}^2\mu_{IS} & {\nu_{IS}}^2\mu_{IS} & 0 \\ -{\nu_U}^2\mu_U & 0 & {\nu_U}^2\mu_U \end{bmatrix}$$

Considering that racking systems are generally characterized by regular geometry and structural repetitiveness, it is possible to introduce some simplifying assumptions that reduce the number of variables at stake. Indeed, it is reasonable to assume a direct linear proportionality between the total mass of the rack (structural and stored) and its height, as well as an inverse linear proportionality between structural stiffness and rack height. The latter assumption is due to the specific geometry of the rack in the cross-aisle direction; indeed, the structural deformation in this direction is mainly controlled by the stiffness of the bracing system (diagonals and crosspieces), which, as known, can be schematized by an equivalent beam shear stiffness.

Based on these assumptions, ν_U and μ_U can be related to each other as expressed in Eq. (6), where h_L and h_U represent the total height of the racking parts respectively below and above the LLIS. Furthermore, the equivalent damping ratios ξ_L and ξ_U can be assumed equal to 0.03, which is the conventional value provided in EN16681 (CEN [24]) for the design of steel storage systems. Therefore, the remaining free variables are ξ_{IS} and ν_{IS}, and the mass ratios μ_{IS} and μ_U. The former are the parameters to be tuned, whereas the latter are the design variables; that is, the values of ξ_{IS} and ν_{IS} that optimize the rack seismic performance will be sought for a wide range of combinations of the isolated mass (μ_{IS}) and its position inside the rack (through the parameter μ_U).

$$\nu_U = \frac{\omega_U}{\omega_L} = \frac{\sqrt{k_U/m_U}}{\sqrt{k_L/m_L}} \approx \sqrt{\frac{h_L^2}{h_U^2}} \approx \sqrt{\frac{1}{\mu_U^2}} = \frac{1}{\mu_U} \quad (6)$$

3. Optimization approach in frequency-domain

3.1. Optimization problem and objective function (OF)

Various TMD optimization models are currently available in the literature, which are based on different structural performance optimization methods. Some of these maximize the effect of the TMD (e.g., Sadek [36]) or the energy dissipated by it (e.g., Reggio and De Angelis [37]); others minimize a given structural response (e.g., Moutinho [38]; Pietrosanti et al. [39]); and still others minimize the response of the primary structure while controlling the drift or acceleration of the isolation (e.g., Bernardi et al. [40]). However, the above models are based on reduced equivalent 2DOF systems (where the primary structure is represented by one DOF). Therefore, for the purpose of LLIS design, a specific optimization model must be appropriately derived.

Based on the dimensionless parameters of the simplified dynamic system, it is possible to define its dimensionless frequency response functions (FRFs), which express how a generic sinusoidal input signal, of a given frequency ω, is transferred within the system. Specifically, the vector $\mathbf{G}(\rho)$ of the dimensionless displacement FRFs is defined as:

$$\mathbf{G}(\rho) = -\left(-\rho^2\mathbf{M}^{/} + i\rho\mathbf{C}^{/} + \mathbf{K}^{/}\right)^{-1}\mathbf{M}^{/}\boldsymbol{\tau} \quad (7)$$

where ρ ($=\omega/\omega_L$) is the ratio between the input (ω) and the lower structure (ω_L) angular frequencies, and $\boldsymbol{\tau}$ is the unit rigid displacement vector [1,1,1].

To model the stochastic nature of the seismic input, the Power Spectral Density (PSD) function of a zero-mean Gaussian stochastic process, $\mathbf{S}(\omega)$, is generally considered. Then, assuming the seismic excitation as a white noise process, the dependence of $\mathbf{S}(\omega)$ on ω can be removed (i.e., $\mathbf{S}(\omega) = S_0$). In this way, ξ_{IS} and ν_{IS} can be calculated by minimizing the variance (σ_d^2) of the displacement response of the simplified system, which is equivalent to minimizing the following integral:

$$\frac{{\boldsymbol{\sigma}_d}^2}{S_0/\omega_L^4} = \int_0^\infty |\mathbf{G}(\rho)|^2 d\rho \quad (8)$$

In particular, optimization of the seismic performance of the rack is pursued by minimizing the displacement variance of the mass m_U (i.e., $\sigma_{d,3}^2$), which is provided by the third component (G_3) of the vector $\mathbf{G}(\rho)$. Therefore, the objective function (OF_d) and the optimization problem are defined as follow:

$$OF_d = \frac{{\sigma_{d,3}}^2}{S_0/\omega_L^4} = \int_0^\infty |G_3(\rho)|^2 d\rho \quad (9)$$

$$J_d : \begin{cases} \min\limits_{\xi_{IS},\nu_{IS}} \left[OF_d(\xi_{IS}, \nu_{IS}, \mu_U, \mu_{IS})\right] \\ subjected\ to \begin{cases} 0 < \xi_{IS} \le 1 \\ 0 < \nu_{IS} \le 1 \end{cases} \end{cases} \quad (10)$$

The variance of the isolation drift ($\sigma_{d,IS}^2$) can also be evaluated through the following equation, where G_1 and G_2 are the dimensionless FRFs of the lower and isolated DOFs, respectively:

$$\frac{{\sigma_{d,IS}}^2}{S_0/\omega_L^4} = \int_0^\infty |G_2(\rho) - G_1(\rho)|^2 d\rho = {\sigma^{/}}_{IS} \quad (11)$$

Optimization of the LLIS parameters is performed parametrically, analyzing many equivalent 3-DOF systems defined by combining various values of μ_{IS} and μ_U. Both parameters range from 0 to 5, with step $\Delta\mu = 0.1$, which represents a sufficiently wide range for these applications (as will be seen later).

Setting $\mu_U = 0$ corresponds to placing the LLIS at the top of the rack; in this case, the 3-DOF model is further simplified, reducing into the

conventional 2-DOF system generally adopted in TMD approaches. Instead, the specific situation with $\mu_U = \mu_{IS} = 0$ corresponds to a rack without LLIS, modeled by a single DOF (i.e., the lower DOF). The latter case is used as a reference, only for convenience, to normalize the values of the objective function:

$$OF_{d,norm} = \frac{OF_d(\mu_U, \mu_{IS})}{OF_d(\mu_U = \mu_{IS} = 0)} \tag{12}$$

3.2. Optimization results

The results of the optimization problem are shown in Fig. 2, linearly interpolated by surfaces for clarity of representation. Specifically, Fig. 2a shows the values of $OF_{d,norm}$, minimized for all μ_U-μ_{IS} combinations; Fig. 2b shows the corresponding values of σ'_{IS}; lastly, Fig. 2c and d show the associated values of $\xi_{IS,opt}$ and $\nu_{IS,opt}$, respectively, which optimize structural seismic performance.

The following considerations can be drawn from these results.

- The $OF_{d,norm}$ values (Fig. 2a) decrease very quickly as μ_U decreases, i.e., the LLIS is much more effective when placed at the upper levels of the rack, as might be expected. In addition, μ_{IS} plays a significant role in reducing the seismic response for high μ_U values only, i.e., when the LLIS is positioned at the lower levels of the rack. Indeed, when the LLIS is placed in the upper part of the rack, its parameters can be effectively tuned, even varying greatly as a function of μ_{IS} to maintain optimal structural control (see Figs. 2c-d for low μ_U values). Conversely, as the LLIS is significantly lowered, its control action is strongly reduced and thus the corresponding optimization leads to pure isolation solutions of the specific LL, which are little affected by μ_{IS} (see Figs. 2c-d for high μ_U values).
- The σ'_{IS} values (Fig. 2b) show peaks in the area with large μ_U and small μ_{IS}, and vice versa, with small μ_U and large μ_{IS}. The first case concerns LLISs placed at the bottom of the rack with low isolated mass ratios, and thus is of little interest; in this case, the peak of the isolation drift variance is explained by the low associated values of optimal damping (see Fig. 2c for high μ_U values). Instead, the second smaller peak of σ'_{IS} concerns LLISs installed at the top of the rack, and is due to the reduction of the frequency ratio ν_{IS} as the isolated mass ratio increases (see Fig. 2d for low μ_U values); this is necessary to control the mass damping effect of the LLIS and achieve the best structural control.
- Figs. 2a-b clearly show that LLIS is most effective in the range of low μ_U-μ_{IS} mass ratios, e.g., between 0 and 2. Indeed, larger μ_U values are associated with increasingly greater overall rack displacements (i.e., $OF_{d,norm}$), and larger μ_{IS} values require increasingly higher-performance isolation systems, due to the greater load to be supported and the greater drift demand (i.e., σ'_{IS}) to be accommodated.

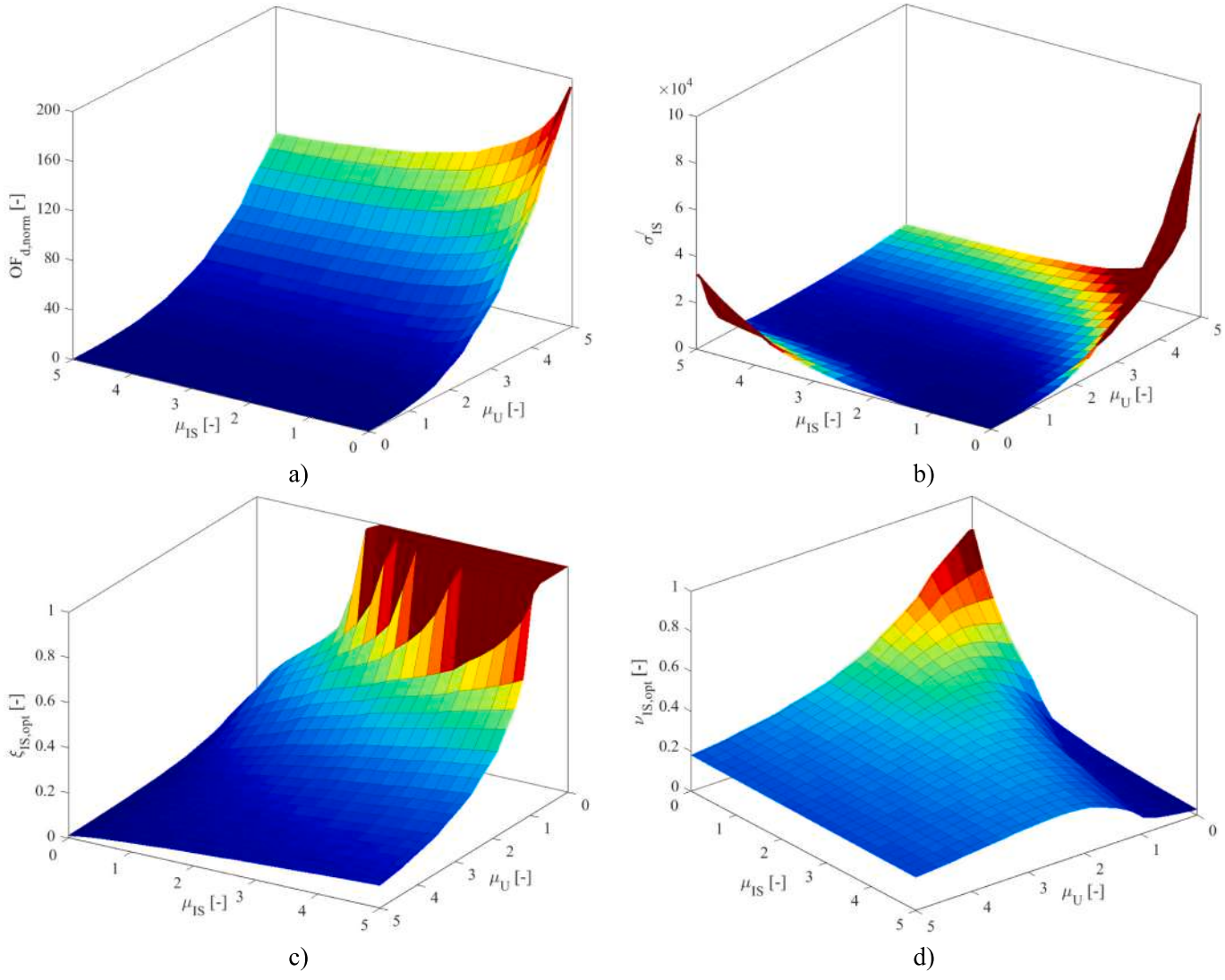

Fig. 2. Optimization results: a) normalized objective function ($OF_{d,norm}$); b) variance of isolation drift (σ'_{IS}); c-d) optimal LLIS parameters ($\xi_{IS,opt}$ and $\nu_{IS,opt}$).

Therefore, the μ_U-μ_{IS} range investigated here is sufficiently wide and, for a more refined search of the optimal LLIS solutions, will be limited between 0 and 2 (see next subsection).

- Regarding the optimal LLIS parameters (Figs. 2 c-d), as already anticipated, for high μ_U values the values of $\xi_{IS,opt}$ and $\nu_{IS,opt}$ are little dependent on μ_{IS} and are comparable with conventional seismic isolation parameters (except for the lowest values of μ_{IS}, where $\xi_{IS,opt}$ tends to 0). Then, as μ_U decreases to values close to 1, both values of $\xi_{IS,opt}$ and $\nu_{IS,opt}$ gradually increase, increasing the control action of the LLIS as its position goes up (i.e., the LLIS begins to behave as an

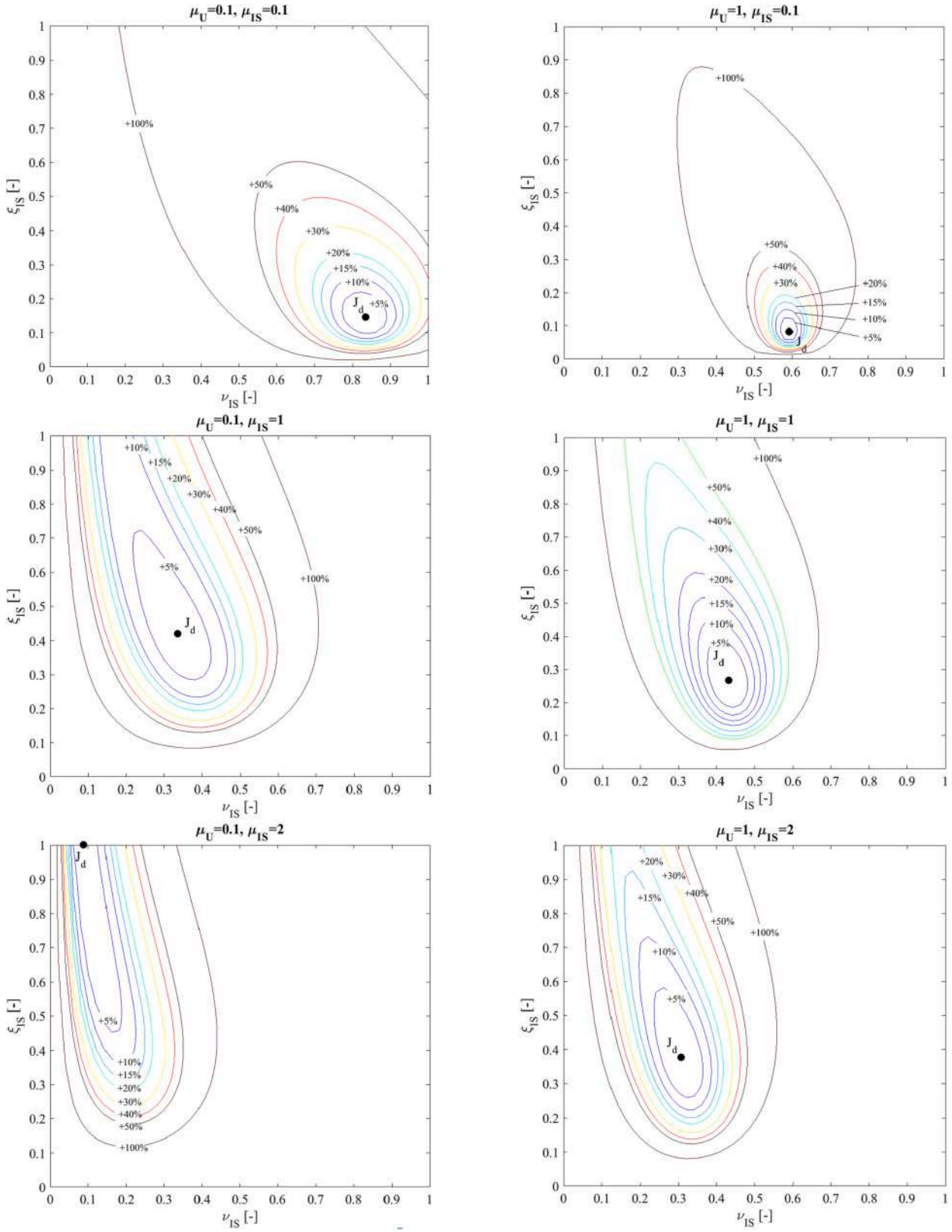

Fig. 3. % increase in $OF_{d,norm}$ over J_d as ν_{IS} and ξ_{IS} change from optimal values, for some cases μ_U-μ_{IS}.

unconventional TMD). Lastly, for μ_U values <1, the values of $\xi_{IS,opt}$ and $\nu_{IS,opt}$ become very dependent on μ_{IS} (as mentioned above). In this situation, the LLIS provides the maximum interaction with the rack. For low μ_{IS} values, this strong interaction is achieved through an increase in both $\xi_{IS,opt}$ and especially $\nu_{IS,opt}$ (for μ_{IS} values close to 0, $\nu_{IS,opt}$ approaches 1); whereas, for high μ_{IS} values, this interaction is obtained by greatly increasing the values of $\xi_{IS,opt}$ and drastically reducing those of $\nu_{IS,opt}$ (for μ_{IS} values >2, $\xi_{IS,opt}$ reaches the critical damping, while $\nu_{IS,opt}$ tends rapidly to 0). This is necessary to provide sufficient dynamic control action while limiting the inertial forces involved.

4. Cost-effective solutions for the LLIS

4.1. Sensitivity analysis

Considering that the costs of industrial racks are generally much lower than those of ordinary building structures, control devices for the former should have very limited costs, as should base isolation systems (e.g., Simoncelli et al., [32]) and other mitigation systems (e.g., Shaheen and Rasmussen [31]) currently proposed for racks. Although a direct comparison of the costs of devices and racking may question the cost-effectiveness of the former, such an evaluation should include all expected seismic losses (direct and indirect), which are highly dependent on the type of production activity, local seismicity, and the vulnerability of storage systems. Although the cost-effectiveness analysis of the LLIS is beyond the scope of this paper, this section intends to provide some assessments for limiting the potential cost of this control system through a sensitivity analysis.

This analysis aims to evaluate the variability of the objective function values as the values of the LLIS parameters change from the optimal ones, $\xi_{IS,opt}$ and $\nu_{IS,opt}$, i.e., from the minimum point reached in the optimization problem (J_d). Specifically, $OF_{d,norm}$ values are calculated for various combinations of ξ_{IS} and ν_{IS}, assumed in the range 0–1, for various cases of μ_U-μ_{IS}. Fig. 3 shows some results of this sensitivity analysis, for μ_U cases of 0.1 (left) and 1 (right), and $\mu_{IS} = 0.1$, 1, 2 (from top to bottom). Each of these graphs shows, in addition to the optimal point (J_d), the percentage increase of $OF_{d,norm}$ over J_d (from 5% to 100%), via isoincrease contour lines.

The results of this analysis clearly show how the objective function is increasingly less sensitive to the change in damping ratio as μ_{IS} increases, especially for low values of μ_U (i.e., with LLIS placed at the top). Indeed, for high values of μ_{IS} and low values of μ_U, the isoincrease intervals of $OF_{d,norm}$ become significantly elongated along the damping axis.

This is very interesting, as the optimization solutions of the top-positioned LLIS are very dissipative (as seen in Fig. 2c for μ_U tending to 0) and therefore difficult to implement. Therefore, the results of this sensitivity analysis suggest that it is reasonable, if not appropriate, to assume damping values less than $\xi_{IS,opt}$ for these cases, designing more feasible and cost-effective isolation devices without significantly reducing the rack seismic performance.

4.2. Cost-effective LLIS parameters

Seismic isolation technologies suitable for LLIS are those used for lightweight structures (such as building contents or laboratory equipment), because of the low loads involved (about 1–3 t per LL and span). Of these, those based on sliding and rolling support systems are certainly more advantageous, allowing the isolation period to be selected regardless of the amount of isolated mass (Kelly [41]). However, these systems do not generally provide very high damping levels; high damping demands could therefore be a discriminating factor in the choice of isolation technology, or require the use of auxiliary dissipation devices. Therefore, it can be stated that the required level of damping is strongly, though not directly, related to the cost of the control system.

In a preliminary study on LLIS, Bernardi et al. [42] investigated the use of the Rolling-Ball Rubber-Layer (RBRL) isolation system (Donà et al. [43]), after appropriate calibration of its parameters. Among the strengths of this isolator are its low implementation costs and great versatility; on the other hand, the ξ_{IS} values achieved by this system were quite low, slightly <10% for the specific application. Despite this, the control system proved effective in enhancing the seismic performance of the rack, leaving ample room for improvement in the case of adopting auxiliary dissipation devices, and thus more expensive control systems.

Therefore, based on the results of the sensitivity analysis, this section aims to derive LLIS tuning solutions that are not only technically effective but also cost-effective. For this purpose, the minimization study defined in Eq. 13 is conducted, which searches for the minimum value of ξ_{IS} for each μ_U-μ_{IS} combination analyzed, such that the value of $OF_{d,norm}$ does not exceed a certain increment from the optimization solution (J_d). Specifically, two increments, 10% (J_d') and 20% (J_d''), were set, corresponding to different levels of damping, both more favorable than that of J_d. Once the minimum values of ξ_{IS} satisfying the above conditions have been identified, the associated values of ν_{IS} can be derived.

$$\begin{aligned} &min \text{ of } \xi_{IS} \text{ s.t. :} \\ &\begin{cases} J_d' : OF_{d,norm}(\xi_{IS},\nu_{IS}) \le 1.1\ OF_{d,norm}(J_d) \\ J_d'' : OF_{d,norm}(\xi_{IS},\nu_{IS}) \le 1.2\ OF_{d,norm}(J_d) \end{cases} \\ &\text{in the range } 0 < \xi_{IS},\nu_{IS} \le 1 \end{aligned} \tag{13}$$

Fig. 4 shows these less damping-demanding solutions (J_d' and J_d''), comparing them with the optimization solutions derived in Section 3 (J_d), both in terms of ξ_{IS} and ν_{IS}. It is clear from this comparison that it is possible to significantly reduce the damping demand in the range of low μ_U values, especially for high μ_{IS} values, while keeping the objective function values close to the optimization values. Considering also that the associated increase in ν_{IS} is small, it can be concluded that the J_d' and J_d'' solutions are potentially much cheaper than the optimization solutions (J_d).

It should also be noted that the reduction in damping level is very high between J_d and J_d', whereas it is much smaller between J_d' and J_d'', with the same reduction step (10%) in the rack seismic performance. Therefore, less performing solutions than J_d'', potentially even cheaper, are not considered in this study. However, wanting to opt for even less dissipative solutions than J_d'', for any practical/economic advantages, it is possible to do so while keeping the same frequency solutions as J_d''.

5. Proposal of a design procedure for the LLIS

For design purposes, this section returns the previous cost-effective solutions of the LLIS through simple prediction models. Specifically, the polynomial function in Eq. 14, which depends on μ_U and μ_{IS} only, is calibrated on the ξ_{IS} and ν_{IS} values of both J_d' and J_d'' minimizations. The calibration coefficients are given in Table 1, as well as the goodness-of-fit parameters, while the comparison between analytical models and numerical values is shown in Fig. 5.

$$\begin{aligned} \xi_{IS},\nu_{IS} = {} & c_1 + c_2{\cdot}\mu_U + c_3{\cdot}\mu_{IS} + c_4{\cdot}{\mu_U}^2 + c_5{\cdot}\mu_U{\cdot}\mu_{IS} + c_6{\cdot}{\mu_{IS}}^2 + \\ & + c_7{\cdot}{\mu_U}^3 + c_8{\cdot}{\mu_U}^2{\cdot}\mu_{IS} + c_9{\cdot}\mu_U{\cdot}{\mu_{IS}}^2 + c_{10}{\cdot}{\mu_{IS}}^3 + \\ & + c_{11}{\cdot}{\mu_U}^3{\cdot}\mu_{IS} + c_{12}{\cdot}{\mu_U}^2{\cdot}{\mu_{IS}}^2 + c_{13}{\cdot}\mu_U{\cdot}{\mu_{IS}}^3 + c_{14}{\cdot}{\mu_{IS}}^4 \end{aligned} \tag{14}$$

Based on the above prediction models, the following four-step LLIS design procedure is proposed.

Step 1. Building the finite element (FE) model of the rack and performing the modal analysis to define μ_U and μ_{IS} based on the main mode in the cross-aisle direction. Various configurations of the LLIS (i.e., number and location of isolated levels) can be evaluated and compared at this stage. For this purpose, a simplified but robust way to proceed is to derive the first modal shape, in the cross-aisle direction, of the rack modeled without the isolated mass (i.e., that of the LLIS). This global

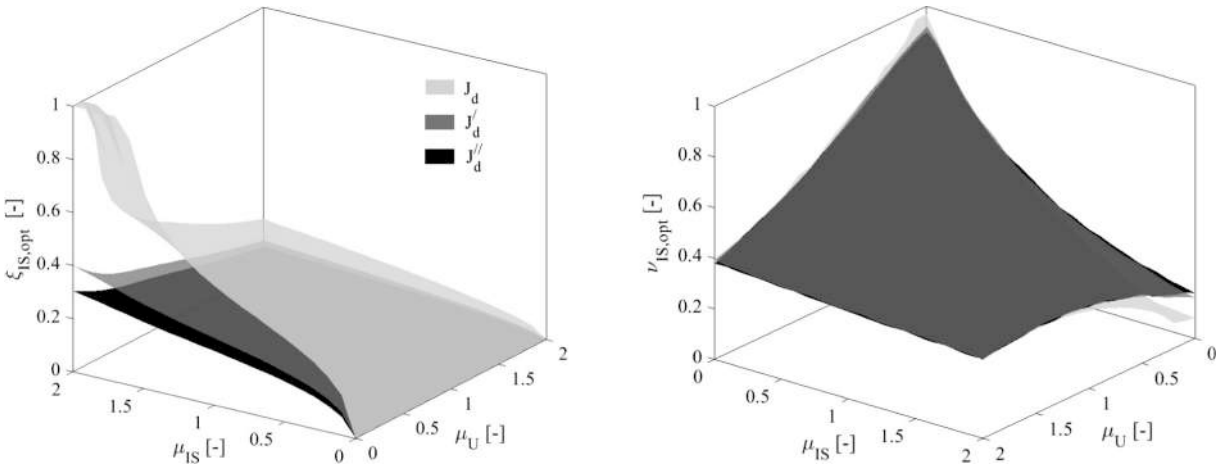

Fig. 4. Cost-effective solutions (J'_d, J''_d) for the LLIS, compared to the optimization solution (J_d).

Table 1
Calibration coefficients and goodness-of-fit parameters of the prediction models.

	J'_d minimization		J''_d minimization	
Coefficients:	ξ_{IS} model	ν_{IS} model	ξ_{IS} model	ν_{IS} model
c_1	0.056	0.919	0.04343	0.9095
c_2	0.001	−0.243	−0.001249	−0.2373
c_3	0.362	−0.909	0.3018	−0.8858
c_4	−0.058	−0.097	−0.04322	−0.09357
c_5	−0.110	0.742	−0.08678	0.7169
c_6	−0.267	0.446	−0.2245	0.4326
c_7	0.024	0.043	0.0178	0.04036
c_8	0.035	−0.109	0.01735	−0.1048
c_9	0.041	−0.336	0.0412	−0.3244
c_{10}	0.119	−0.114	0.09786	−0.1089
c_{11}	−0.022	−0.021	−0.01249	−0.02172
c_{12}	0.020	0.060	0.01135	0.0602
c_{13}	−0.023	0.042	−0.01697	0.03839
c_{14}	−0.017	0.012	−0.01471	0.01135
Fit parameters:				
SSE	0.004	0.008	0.0019	0.0093
R^2	0.998	0.998	0.9988	0.9982
$R^2_{adjusted}$	0.998	0.9984	0.9987	0.9981
RMSE	0.003	0.004	0.0022	0.0048

modal shape can then be used to estimate the first-mode shapes, in the same direction, of the lower and upper parts of the rack (i.e., below and above the LLIS) by separating it just below the LLIS and normalizing the two resulting portions (from 0 to 1). The latter can then be used to derive m_L and m_U via the formulas in Eq. 1. Thus, knowing the isolated mass m_{IS}, it is possible to calculate μ_U and μ_{IS} through the formulas in Eq. 4, for the various LLIS configurations investigated. Alternatively, more precise evaluations can be conducted, requiring the construction and modal analysis of two separate FE rack models, one for the lower part and the other for the upper part of the structural system (for each assumed LLIS configuration).

Step 2. Selection of the LLIS configuration (i.e., μ_U and μ_{IS} values), based on any design requirements and/or technical limitations, or based on the structural performance trends shown in Fig. 6. Specifically, the graphs in this figure provide the trends of $OF_{d,norm}$ and σ'_{IS} as a function of μ_U and μ_{IS}, over the range of interest (i.e., $\mu_U = \mu_{IS} = 0$ to 2). As can be seen, reducing μ_U always reduces the values of $OF_{d,norm}$, but not those of σ'_{IS} for relatively large values of μ_{IS} (>1), where σ'_{IS} shows a trend with concavity.

Step 3. Calculation of the LLIS parameters, ξ_{IS} and ν_{IS}, as a function of μ_U and μ_{IS}, using the prediction models proposed above (see Eq. 14).

Step 4. Performing the modal analysis of the rack part below the LLIS to determine its first circular vibration frequency in the cross-aisle direction (ω_L). Knowing ν_{IS} and ω_L, it is possible to derive ω_{IS} through Eq. 4. Then, also knowing m_{IS}, k_{IS} and c_{IS} constants of the LLIS can be determined through the formulas in Eq. 2.

6. Case study analysis

6.1. Presentation of the case study rack

To evaluate the LLIS effectiveness as a technique for structural vibration control of steel racking systems and to show the application of the proposed design procedure, a case study is presented in this section.

The assumed rack is representative among the single-entry ones used in Italy and designed for static loads only. It consists of eight load levels, with an inter-level height of 1250 mm, and five spans 2700 mm long. The plan dimensions are 13.5 m × 1 m, and the total height is 10.6 m. Each pair of pallet beams supports a total weight of 2.1 *t* (i.e., three pallets of 700 kg each). The following structural information was provided by a major Italian manufacturer of such systems.

Frames in the cross-aisle direction are composed of two uprights, braced by diagonal and horizontal members connected to the uprights by bolted hinge joints. In the down-aisle direction, the uprights are connected by pallet beams via semi-rigid connections, with rotational stiffness ($k_{\varphi,Y}$) of 1.17•10^8 N•mm/rad. The base connections of the uprights are bolted in such a way as to create a hinge joint along the cross-aisle direction (i.e., around the *X* axis) and a semi-rigid joint along the down-aisle direction (i.e., around the *Y* axis), with rotational stiffness (k_{φ,Y_base}) of 4.35•10^8 N•mm/rad.

All rack elements are thin-walled open-section steel profiles (see Fig. 7). The upright cross-section has dimensions 100x87x2 mm (Fig. 7a), the diagonal/horizontal frame elements are C-profiles with plan dimensions 20x35x9.5 × 1.2 mm (Fig. 7b), and the pallet beams are coupled C-profiles, each of size 100x50x9x1.5 mm (Fig. 7c). The effective inertial properties of these cross sections, i.e., area (*A*) and moments of inertia in the main directions (J_x, J_y, J_z), and the elastic modulus of steel are given in Table 2. Specifically, the uprights are made of S350-type steel, the frame bracing elements of S250GD steel, and the pallet beams of S275JR steel.

The structure is modeled using MidasGen software (MidasGen [44]), and its model is shown in Fig. 8. Elastic beam elements are used for uprights and pallet beams, whereas truss elements are used for diagonal and horizontal frame elements. The warping effect (Bernuzzi et al. [45]) is taken into account for uprights, via a specific command available in the software. The beam-to-upright and base connections are modeled as hinges with the rotational stiffnesses mentioned above ($k_{\varphi,Y}$ and k_{φ,Y_base}, respectively). The pallet mass is modeled as a lumped mass, positioned

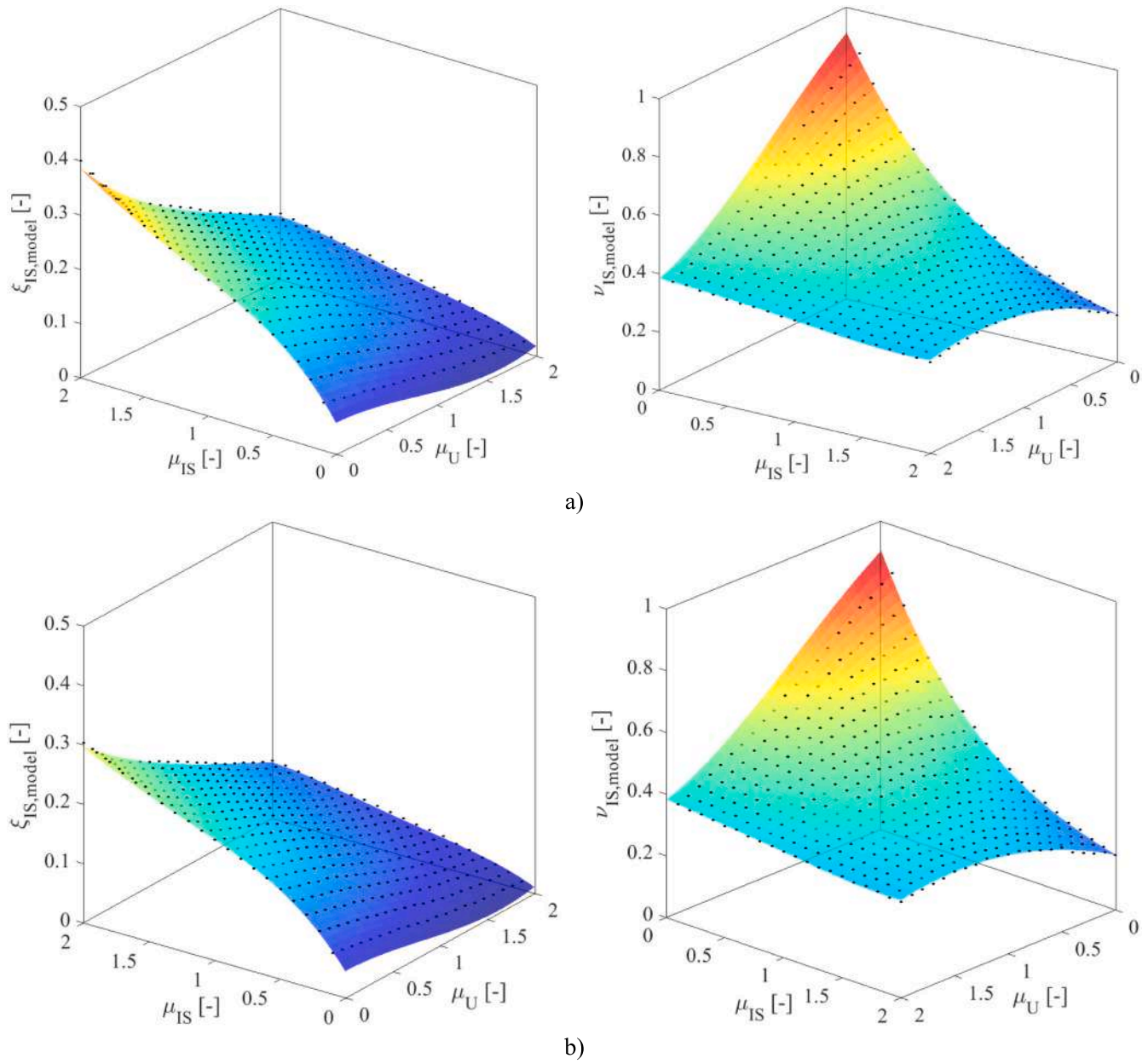

Fig. 5. Prediction models of ξ_{IS} and ν_{IS} for the LLIS cost-effective solutions: a) J_d'; b) J_d''.

in the center of each load level and raised above it to account for the pallet's actual center of gravity. According to EN 16681 (CEN [24]), a dummy substructure is adopted to connect this mass to the rack structure, consisting of four sufficiently rigid truss elements arranged in a pyramid scheme (see Fig. 8). Fig. 9 shows the main modal results for the first three vibration modes of the rack.

6.2. Design of the LLIS

First, it is necessary to calculate the μ_U and μ_{IS} mass ratios of the equivalent 3-DOF system. These can be obtained as described in Section 2, with reference to the first vibration mode of the rack in the cross-aisle direction. Three LLIS configurations were assumed in this study, corresponding to the isolation of one of the three highest load levels (i.e., 8th, 7th, and 6th LL). As an example, Fig. 10 shows the derivation of μ_U and μ_{IS} for the case with LLIS placed at the 6th LL.

Then, the main steps to derive the optimal-effective LLIS parameters are summarized in Fig. 11, with their partial results. The first step precisely provides the μ_U and μ_{IS} values for the various LLIS configurations. In the second step, the results in Fig. 6 are used to select the desired LLIS configuration, based on μ_U and μ_{IS}. In this study, assuming no design requirements or constraints, the case with the lowest $OF_{d,norm}$ is chosen, i.e., the one with the LLIS at the top. In any case, the other LLIS configurations are also analyzed in the next subsection for comparison purposes. In the third step, the proposed prediction models for J_d' minimization (Eq. 14, Table 1) are employed to derive the optimal values of ξ_{IS} and ν_{IS} based on μ_U and μ_{IS}. Lastly, in the fourth step, the stiffness (k_{IS}) and damping (c_{IS}) constants of the LLIS are calculated based on the values of ξ_{IS}, ν_{IS} and ω_L.

Therefore, for the subsequent TH analyses, the LLIS is modeled by Kelvin elements (i.e., linear spring in parallel to linear dashpot) with k_{IS} and c_{IS} constants, which act along the cross-aisle direction and are placed between the top of the dummy substructures and the pallet masses in the isolated LL.

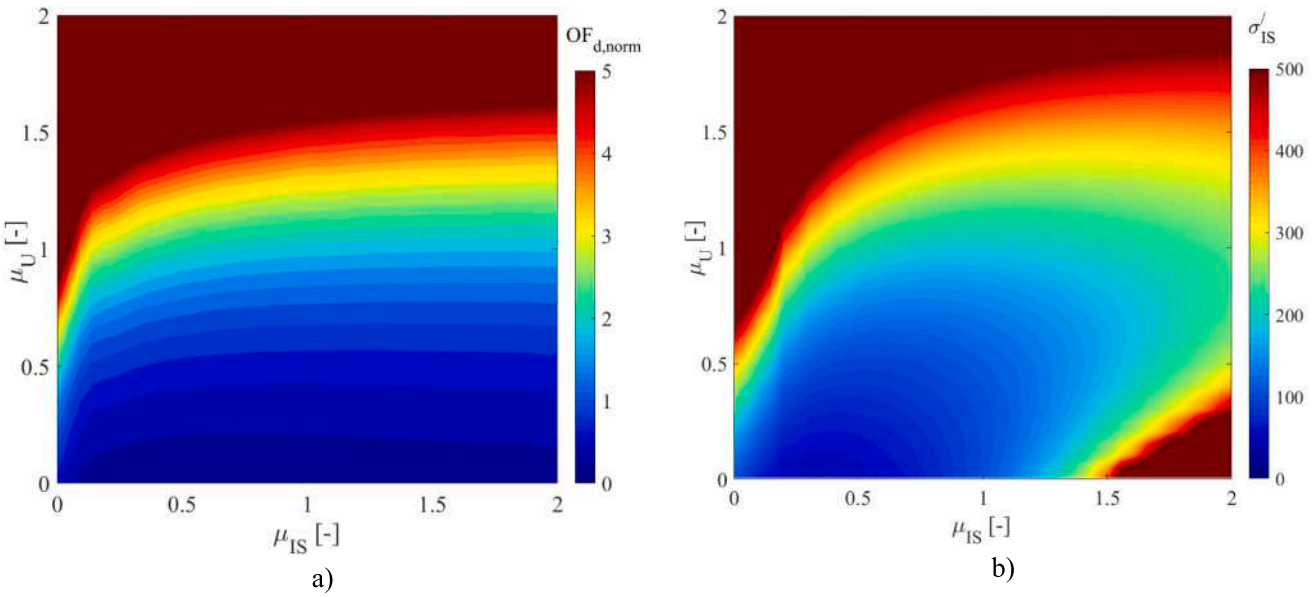

Fig. 6. Optimization values of (a) $OF_{d,norm}$ and (b) σ'_{IS} as a function of μ_U and μ_{IS}.

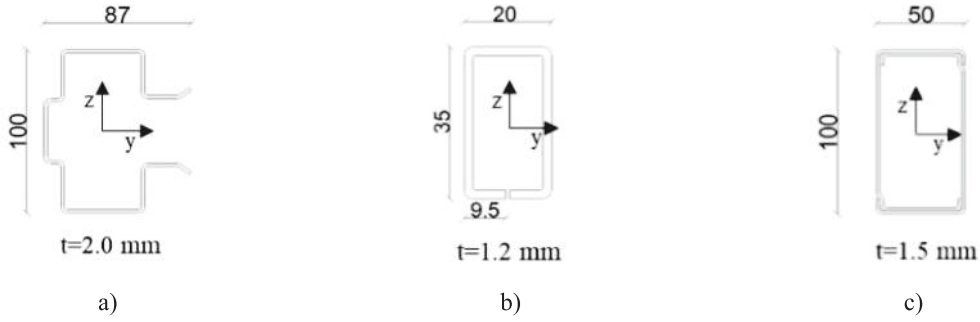

Fig. 7. Cross sections of: (a) uprights; (b) diagonal/horizontal frame elements; (c) pallet beams.

Table 2
Inertial properties of the cross sections of the rack profiles.

	A [cm^2]	J_x [cm^4]	J_y [cm^4]	J_z [cm^4]	E [MPa]
Uprights	5.44	0.08	62.00	37.00	210,000
Frame bracing elements	1.2	0.01	1.86	0.8	210,000
Pallet beams	7.22	95.14	162.4	30.5	210,000

6.3. Seismic analysis and effectiveness of LLIS

For the TH analyses, seven bidirectional natural records were selected from the SIMBAD Database using REXEL (Iervolino et al. [46]). These records were scaled to be compatible (on average) with the Type 1 elastic response spectrum of EC8 (CEN [47]), defined assuming a bedrock acceleration of 0.25 *g* and a type B soil, resulting in a peak ground acceleration of 0.3 *g*. The main details of these events are reported in Table 3, and the related acceleration spectra are shown in Fig. 12, together with the EC8 reference spectrum.

The effectiveness of the LLIS is evaluated by comparing the TH results of the cases without control system and with control system placed at the 8th LL. Figs. 13 to 15 show these results in terms of maximum absolute displacements along the rack height (Fig. 13), maximum absolute forces at the base of the uprights (Fig. 14), and maximum absolute accelerations on the pallet masses (Fig. 15).

Specifically, Fig. 13 shows the maximum displacement profiles of the upright located in the middle of the rack, recorded in the cross-aisle direction under the various seismic events. This figure also displays the average displacement profiles among those of the various events, for both cases with and without LLIS. These comparisons prove the significant dynamic control of the LLIS in the cross-aisle direction, which increases as the load level increases, resulting in a 60% reduction in rack top displacement. In addition, a beneficial reduction in variability in the displacement response can be observed when using LLIS. Clearly, in the down-aisle direction there is no appreciable change in the displacement profiles between the cases with and without LLIS, and therefore these results were not shown.

Fig. 14 shows the maximum forces recorded at the base of all uprights, indicating by "A" and "B" the two rows of uprights in the down-aisle direction, and by numbers 1 to 6 the frames in the cross-aisle direction. Specifically, Fig. 14a shows the axial compression forces, and Figs. 14b the shear forces in the transverse direction. The main observations on these graphs are given below.

- The LLIS leads to a significant reduction in the axial force on the uprights and thus in the probability of collapse of the racking when subjected to seismic actions; for this case study, where these forces are fairly evenly distributed, the reduction achieved by applying the LLIS to the eighth LL, averaged across all uprights, is about 60% (see Fig. 14a).
- Shear forces at the base of the uprights in the cross-aisle direction are also greatly reduced with the application of the LLIS, by 47% on average among all uprights (see Fig. 14b). In addition, these results show a more demanding force distribution for row B of uprights, compared to

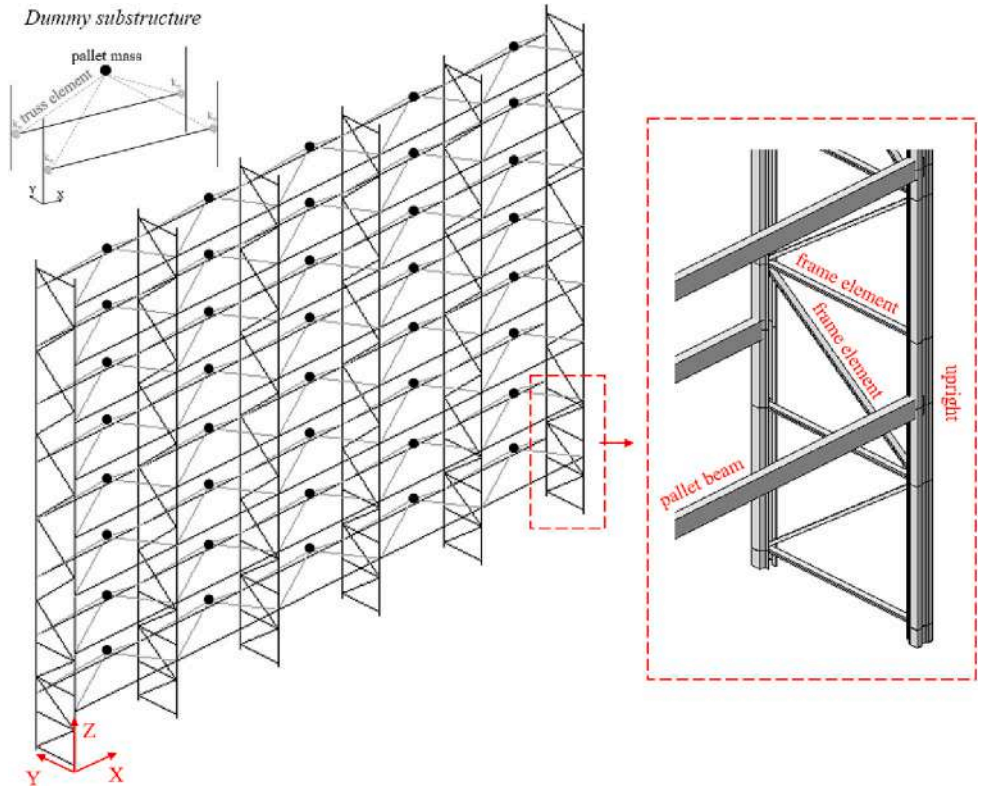

Fig. 8. FE model of the case study rack.

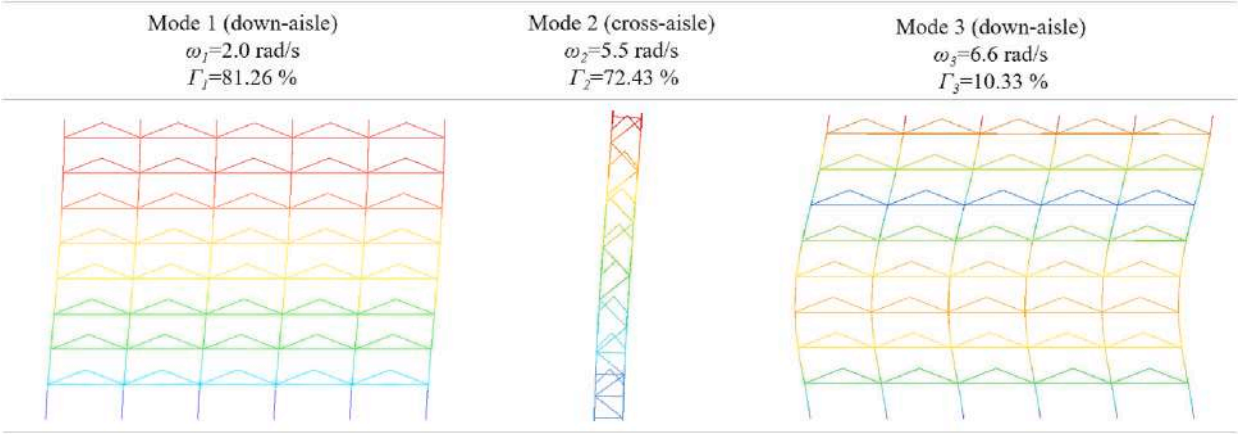

Fig. 9. Main vibration modes of the rack, and related frequencies (ω_i) and participation factors (Γ_i).

row A, justified by the specific arrangement of diagonals in the frames, as well as a slight increase in these forces from outer to inner frames.

Therefore, considering the results in Figs. 13 and 14, we can confirm the effectiveness of the control technique and thus its feasibility as a retrofit technique. Indeed, LLIS might be advantageous over traditional retrofit interventions, such as inserting longitudinal bracing and strengthening uprights, which increase the stiffness of the rack and thus potentially its seismic demand.

Fig. 15 shows the maximum accelerations on the pallet masses of the middle span of the rack, for the various LLs, in the cross-aisle direction. It is worth noting that a significant reduction of these accelerations is obtained not only at the isolated level, but also at the other LLs. Specifically, the maximum acceleration without the LLIS is reached at the top of the rack, and is 0.87 g; with the LLIS, this is reduced to 0.55 g, and reached at the seventh LL. Furthermore, the top acceleration reduction is 36%.

The reduction in accelerations allowed by the LLIS also makes it very attractive as a seismic mitigation technique for newly designed racking. Indeed, although there are seismic standards (e.g., EN16681, CEN [24]) to design earthquake-proof racks, the stability of stored goods remains an open issue, particularly in areas of high seismicity. In fact, the high accelerations at the upper LLs of medium-to-high rise racks, especially when stiffened to support high seismic forces, can cause stored goods to fall, posing a threat to the safety of people and the production continuity of companies. The only way to reduce these accelerations is to intervene in the dynamics of these systems by inserting dissipators (e.g., Shaheen and Rasmussen [31]) and/or isolation systems (e.g., Simoncelli et al. [32]). The latter can be implemented at the base of the structure or, precisely, through the LLIS technique, which as mentioned in the Introduction has some advantages over base isolation, such as greater

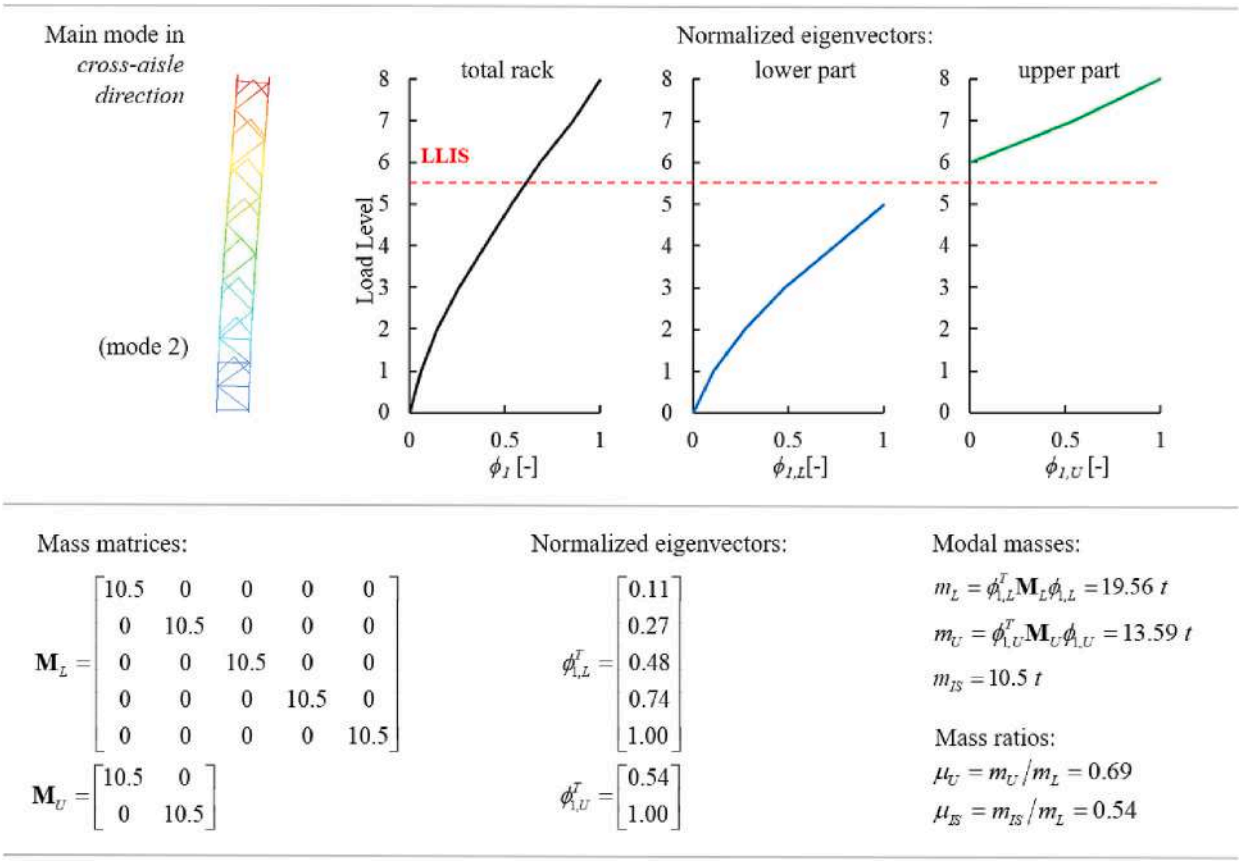

Fig. 10. Example of calculation of μ_U and μ_{IS} for the case study with LLIS at the 6th LL.

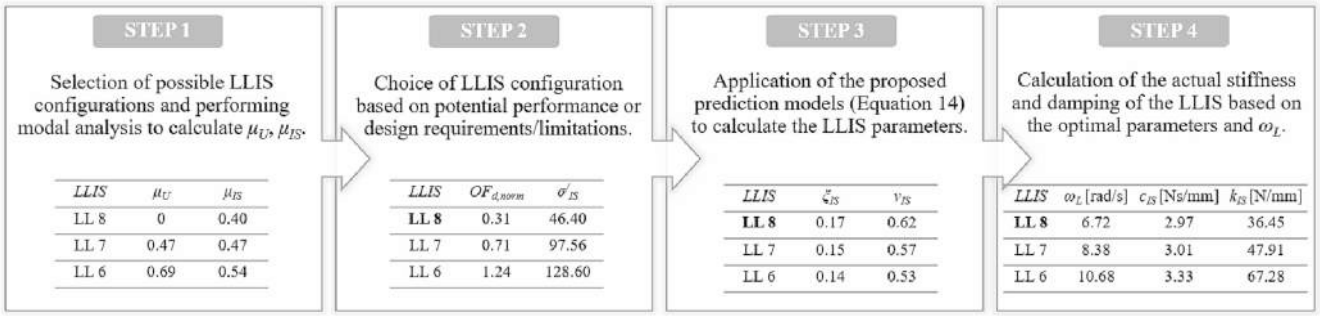

Fig. 11. Main steps to derive the optimal-effective LLIS parameters.

simplicity of design (less dependence on pallet mass distribution), less or no interference with goods handling operations and greater ease of installation (especially in existing rack systems).

Table 4 compares, for all LLIS configurations analyzed, the maximum rack top displacements (d_{MAX}), the maximum pallet accelerations (a_{MAX}, with the LL of record), and the maximum isolation deflection (d_{IS}). All these values are still obtained as an average over the seven bidirectional events. The results in this table confirm that lowering the position of the LLIS increases the overall seismic response of the rack (i.e., both d_{MAX} and a_{MAX} values), while, on the other hand, the displacement demand of the isolators (d_{IS}) is reduced. Therefore, in general, although the best seismic performance of the rack would be achieved with the LLIS positioned at the top, a different LLIS configuration could be chosen, based on a case-by-case evaluation of the possible technical limitations of the devices, their costs, and other design requirements, which, however, is beyond the scope of this study.

6.4. *Effect of damping level on structural system response and final remarks*

Lastly, it is interesting to evaluate the effect of the damping level on the response of the structural system. To this end, a specific parametric TH analysis was conducted, using the case study rack with LLIS placed at the 8th LL, and setting the value of ξ_{IS} to 0.05, 0.1, 0.2, 0.3, and 0.4. All other parameters and conditions of analysis remained the same.

The results of this further investigation are shown in Fig. 16a, b, and c, respectively in terms of maximum deflection of isolators (d_{IS}), maximum compression axial force and maximum shear force in the cross-aisle direction at the base of the B3 upright. These results are also compared with those obtained with the J'_d optimization (i.e., $\xi_{IS} = 0.17$).

It is evident from Fig. 16a that d_{IS} decreases as ξ_{IS} increases, as expected. The maximum isolation drift ranges from 250 to 150 mm in the analyzed damping range, displacements all compatible with traditional isolation technologies.

Table 3
Selected bidirectional natural records.

ID	Earthquake	Date	Mw	Epicentral distance [km]	Site class	Scale factor X	Y
eq.1	Eastern Fukushima Prefecture	2011/04/11	6.6	26.24	B	1.30	1.38
eq.2	Imperial Valley	1979/10/15	6.5	24.68	B	1.59	1.48
eq.3	S. Suruga Bay	2009/08/10	6.2	25.38	B	0.60	0.97
eq.4	Friuli 1st shock	1976/05/06	6.4	21.72	B	0.79	0.72
eq.5	Eastern Fukushima Prefecture	2011/04/11	6.6	27.56	B	2.33	1.41
eq.6	Irpinia	1980/11/23	6.9	21.79	B	1.34	1.93
eq.7	Irpinia	1980/11/23	6.9	18.85	B	1.43	1.58

Fig. 16b and c show a concavity trend with the minimum value reached near the optimal solution $J_d^{'}$, reflecting the effectiveness of the proposed optimal solution. Moreover, this trend is more evident for compression forces than for shear forces, indicating a greater effect of ξ_{IS} on the former. This is justified by the importance of the bending moment on the rack, this being a very slender structure in the cross-aisle direction.

In fact, the reduction of ξ_{IS} from the optimal value (i.e., $\xi_{IS} = 0.17$) reduces the interaction between LLIS and rack compared to the optimal situation, and this results in greater lateral/flexural deformation of the rack and thus greater forces at the base of the uprights, mainly in the axial direction.

Instead, the increase in ξ_{IS} from the optimal value increases the interaction between the LLIS and rack compared to the optimal situation, and this leads to higher inertial forces transmitted from the isolated pallet to the 8th LL. Although in this case the high level of dissipation allows the maximum shear forces at the upright base to remain nearly constant, the higher shear force generated in the isolated LL produces an increase in bending moment and thus in the axial force at the base of the upright.

Ultimately, increasing ξ_{IS} beyond the optimal value, in addition to requiring more expensive technological solutions, has the sole benefit of reducing d_{IS}, and may even increase the stress state of the uprights.

As shown in this case study, the best location of the LLIS is generally the top of the rack. This suggests starting to fill the rack from that isolated LL. However, in the case of partial loading of the rack (i.e., only the lower and/or intermediate LLs), the seismic forces, and especially the bending moments, would be lower than those estimated and controlled by LLIS in this case study. Therefore, it is necessary for the isolated LL to be loaded only beyond a certain percentage of rack filling, which was not evaluated in this study and is a topic of interest for future investigation.

An alternative solution to avoid interfering with the logistics of pallet handling would be to use a permanent TMD system on top of the rack; however, this solution would present some other issues. Indeed, when a permanent TMD system is anchored to the rack top, it occupies the storage space of the last LL, thus reducing the storage capacity as well as the effective load-bearing capacity of the rack. Another solution could be a permanent suspended TMD system, i.e., hanging from the roof of the industrial building. In the latter case, the TMD would provide the dynamic control function without interfering with either the logistics of pallet handling or the storage capacity of the rack. However, such a

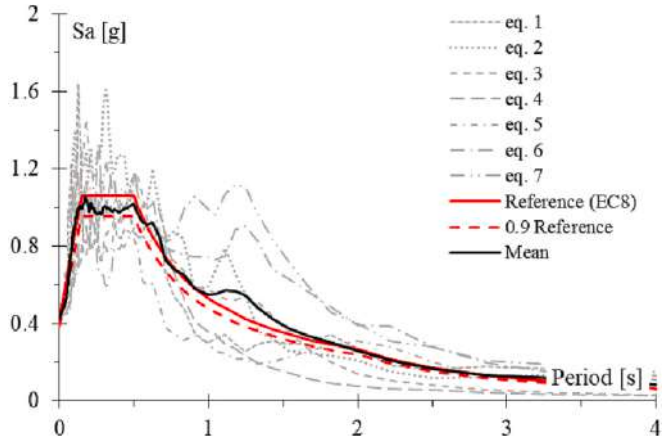

Fig. 12. Acceleration response spectra of the selected events and EC8 reference spectrum.

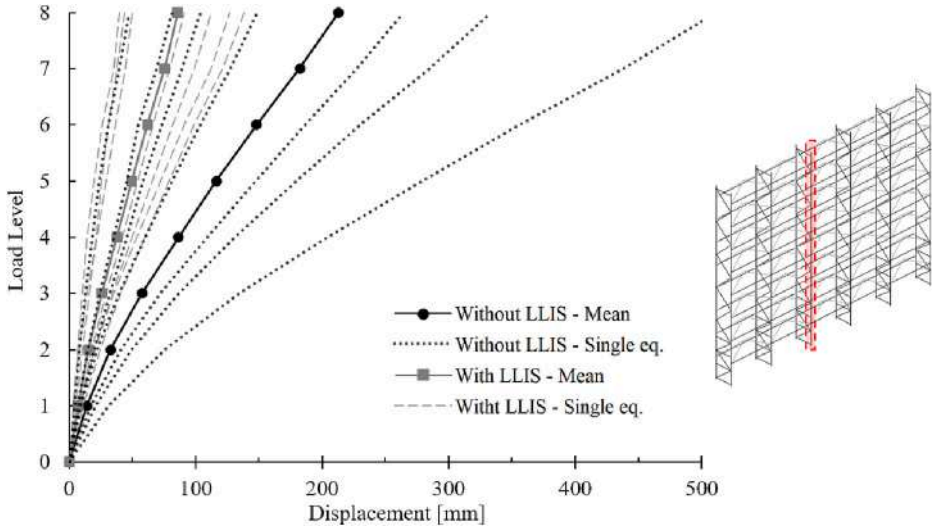

Fig. 13. Maximum displacement profiles of the inner upright in the cross-aisle direction, with and without the LLIS.

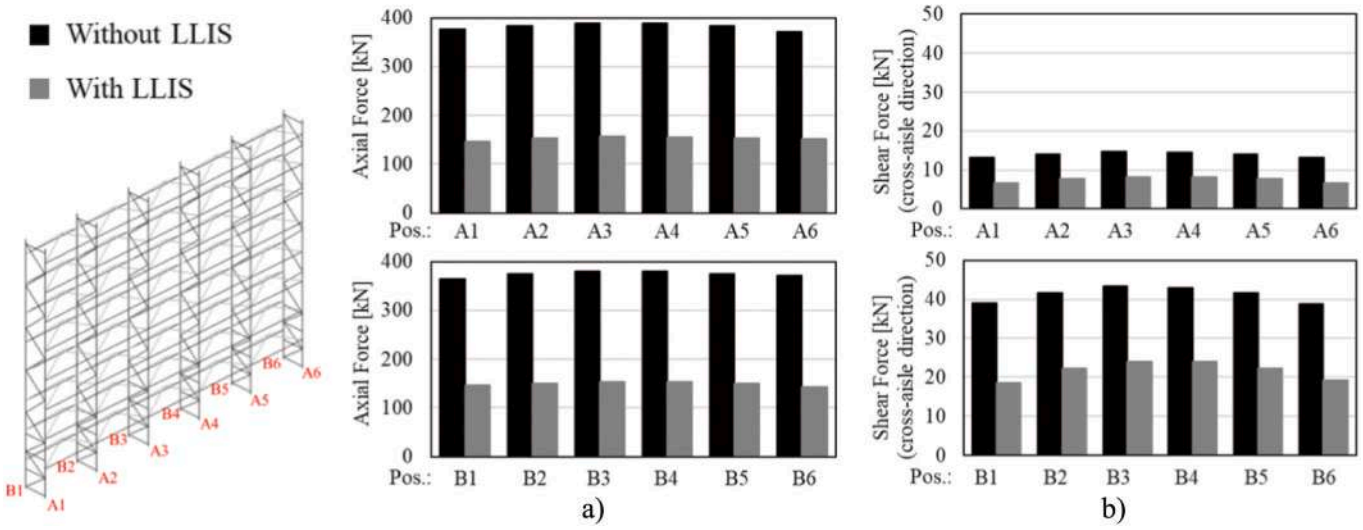

Fig. 14. Maximum forces at the base of all uprights, with and without the LLIS: (a) axial forces and (b) shear forces in the cross-aisle direction.

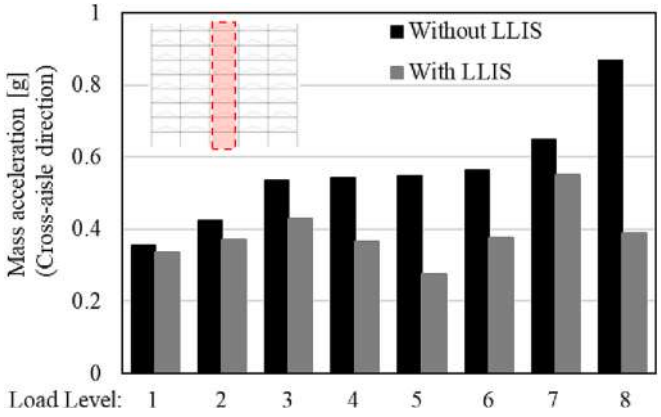

Fig. 15. Maximum accelerations on the pallet masses of the central span, in the cross-aisle direction.

Table 4
Maximum rack top displacements (d_{MAX}), pallet accelerations (a_{MAX}) and isolation deflection (d_{IS}) for all analyzed LLIS configurations.

LLIS position:	d_{MAX} [mm]	a_{MAX} [g]	d_{IS} [mm]
LL 8	85.8	0.55 (LL 7)	196.0
LL 7	101.1	0.64 (LL 8)	193.4
LL 6	137.0	0.62 (LL 8)	171.2

system would be very expensive compared to the relatively low cost of industrial storage facilities.

This case study also demonstrated the effectiveness of LLIS in reducing the peak acceleration of pallets and the entire acceleration profile of LLs in general. Should the pallet accelerations remain high enough to trigger pallet sliding, conventional precautions against pallet falling can also be taken for isolated LLs. These consist of fall arrest systems, such as restraint nets or retaining elements applied to the pallet beams (in the isolated LL, these systems should be applied to the second level of beams making the isolation layer). Another solution is to interpose layers of rough material between the pallets and support beams, so as to increase the relative coefficient of friction and thus the sliding trigger accelerations. Finally, if the previous solutions are not feasible for the specific application or are still not sufficient (e.g., in extreme cases of very high racking systems located in areas of high seismicity), installation of seismic isolation at the base of the rack should also be considered to significantly reduce seismic accelerations entering the structure.

7. Conclusions

This study focused on an innovative control system for dynamic actions on steel racking structures, called Load-Level Isolation System (LLIS), which is based on the use of stored pallet masses as TMDs. Specifically, the LLIS consists of inserting isolators directly between the pallet masses and the load level (LL), in one or more LLs. This study is driven by the need to find increasingly high-performance seismic mitigation solutions for industrial storage systems, which are increasingly popular also due to the growth of the logistics and e-commerce sectors. This need concerns both existing racks, not designed according to anti-seismic criteria (to reduce their damage probability), and newly designed earthquake-proof racks, when located in seismic prone areas (to reduce pallet accelerations).

A preliminary study (Donà et al. [35]) showed the potential of this control technique by directly investigating a case study pallet rack. This earlier study also revealed the need to develop optimal LLIS tuning methods that are sufficiently general, that is, applicable to various storage systems. In this context, this paper aimed to provide a general design method of the LLIS, based on the optimization of its stiffness and damping parameters as a function of the dynamic characteristics of the rack, the amount of isolated mass, and its location within the rack (which are the design variables).

After defining the reduced 3-DOF system representative of the dynamics of the LLIS-equipped rack, a parametric analysis was performed in the frequency domain to optimize the isolation parameters. Specifically, a wide range of case studies was analyzed, in terms of isolated mass (μ_{IS}) and its position within the rack (μ_U). For each of these cases, the optimal LLIS parameters were derived through a single-objective optimization procedure, corresponding to the minimization of the displacement variance of the third DOF (representing the upper part of the rack). The optimization results were then used in a sensitivity analysis to obtain more cost-effective solutions for the LLIS. In particular, two sets of solutions were calculated, which allow to considerably reduce the required damping levels while maintaining seismic performances close to the optimal ones (with a worsening of 10% and 20%, respectively). Therefore, based on the latter solutions, prediction models of the LLIS parameters were calibrated and provided, and a specific design procedure of this control system was proposed. Finally, with the

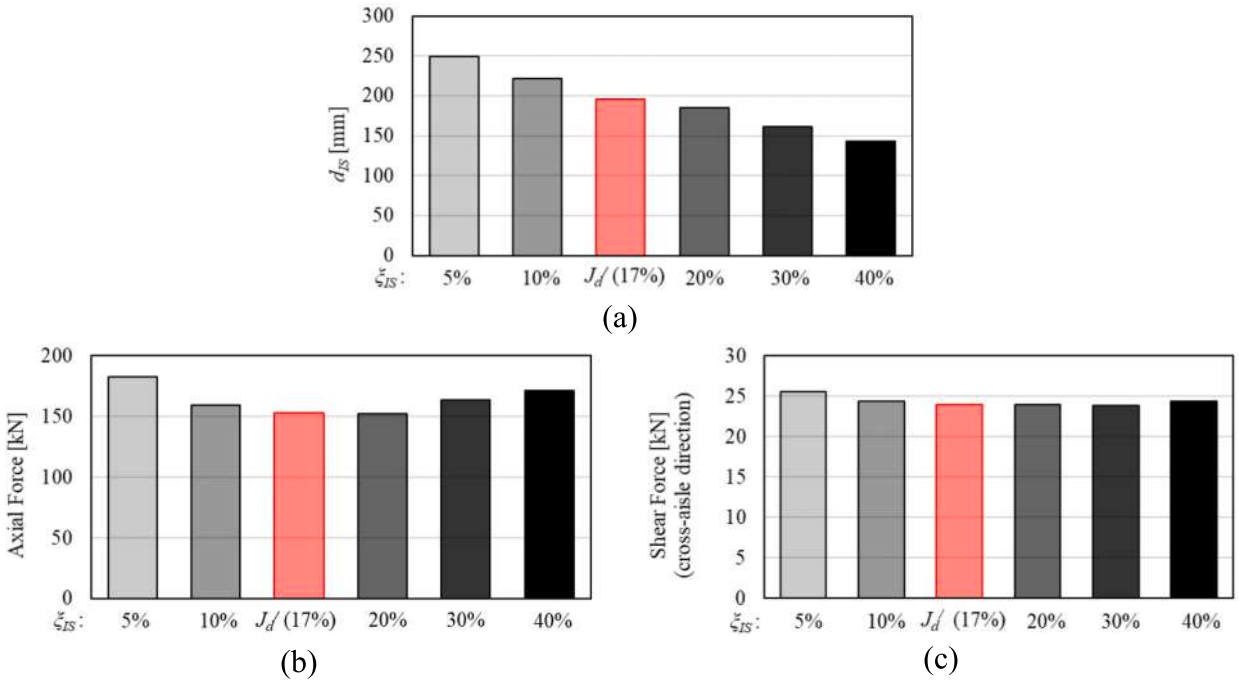

Fig. 16. Seismic performance for incremental damping ratios; maximum values of: (a) isolation drift, and (b) axial forces and (c) shear forces (in the cross-aisle direction) at the base of B3 upright.

aim of showing the application of this design procedure as well as the effectiveness of the LLIS in mitigating seismic effects in a standard pallet rack, a case study was presented. A single-entry rack with five spans and eight load levels was analyzed in TH, subjected to seven bi-directional and spectrum-compatible natural events, in the case with and without LLIS (applied to various LLs).

The main conclusions of this study are given below.

- The effectiveness of the LLIS depends greatly on its position (μ_U), but also on the amount of isolated mass (μ_{IS}), and with reference to the analyses on the equivalent reduced system, it increases both as the LLIS position rises and as μ_{IS} increases (especially for low LLIS placements).
- The optimal values of damping ($\xi_{IS,opt}$) and frequency ($\nu_{IS,opt}$) of the LLIS are comparable with those of conventional seismic isolation systems for low positions of the control system, and they increase as the position of the LLIS rises, thus increasing the control action over the isolation function. In addition, the values of $\xi_{IS,opt}$ and $\nu_{IS,opt}$ become increasingly dependent on μ_{IS} as the LLIS position increases; in particular, as μ_{IS} increases, $\xi_{IS,opt}$ increases and $\nu_{IS,opt}$ decreases, in order to maintain the optimal interaction between LLIS and rack but limiting the inertial forces.
- Sensitivity analysis showed the robustness of the optimal solutions obtained, with respect to the damping parameter ξ_{IS}, for low values of μ_U (i.e., with the LLIS placed on top) and for relatively high values of μ_{IS}. This means that the variation of ξ_{IS} from its optimization value ($\xi_{IS,opt}$) does not greatly affect the values of the objective function. For these cases it is therefore reasonable, if not appropriate, to assume damping values less than $\xi_{IS,opt}$, designing more feasible and cost-effective isolation devices without appreciably reducing the seismic performance of the rack.
- The proposed case study demonstrated the effectiveness of the LLIS technique, showing significant reductions in the displacement profile (up to 60%), shear forces at the base of the uprights (up to 47%) and accelerations on the pallet masses (up to 36%), in the cross-aisle direction, as well as in the axial compression forces on the uprights (up to 60%).
- The case study also confirmed the appropriateness of the proposed design procedure, which makes it easy to evaluate various optimal LLIS configurations (i.e., various placements within the rack) to meet any design requirements or technical limitations of the isolators (especially in terms of maximum deflection).

Future developments involve evaluating the effects of partial rack loading and uneven pallet distribution on the effectiveness of the LLIS technique, to identify possible critical pallet arrangements and provide more comprehensive design guidance. In addition, based on the proposed optimization procedure, it would be meaningful to investigate the cost-effectiveness of the LLIS in probabilistic terms, evaluating the reduction in seismic fragility and risk achievable in various racking systems, and comparing this benefit with the probable LLIS installation cost.

CRediT authorship contribution statement

Enrico Bernardi: Conceptualization, Methodology, Software, Formal analysis, Data curation, Visualization, Writing – original draft. **Marco Donà:** Conceptualization, Methodology, Validation, Data curation, Writing – original draft, Writing – review & editing. **Ping Tan:** Supervision. **Francesca da Porto:** Supervision.

Declaration of Competing Interest

The authors declare that they have no known competing financial interests or personal relationships that could have appeared to influence the work reported in this paper.

Data availability

Data will be made available on request.

Acknowledgements

This work was supported by the National Natural Science Foundation

of China [grant number 51978185]. This study was also carried out within the RETURN Extended Partnership and received funding from the European Union Next-GenerationEU (National Recovery and Resilience Plan – NRRP, Mission 4, Component 2, Investment 1.3 – D.D. 1243 2/8/2022, PE0000005).

References

[1] CEN (European Committee for Standardization), EN 15878 Steel Static Storage Systems – Terms and Definitions. Brussels, 2010.
[2] CEN (European Committee for Standardization), EN 15512 Steel Static Storage Systems – Adjustable Pallet Racking Systems – Principles for Structural Design. Brussels, 2020.
[3] M.S.A. Shaheen, K.J.R. Rasmussen, Development of friction damped seismic fuses for steel storage racks, J. Constr. Steel Res. 192 (2022), 107216.
[4] C. Bernuzzi, M. Simoncelli, An advanced design procedure for the safe use of steel storage pallet racks in seismic zones, Thin-Walled Struct. 109 (2016) 73–87, https://doi.org/10.1016/j.tws.2016.09.010.
[5] CEN (European Committee for Standardization), Design of Steel Structures, part 1-8: Design of joints, in: Eurocode 3, EN 1993-1-8, CEN, Brussels, 2005.
[6] C. Bernuzzi, C.A. Castiglioni, Experimental analysis on the cyclic behaviour of beam-to-column joints in steel storage pallet racks, Thin-Walled Struct. 39 (10) (2001) 841–859, https://doi.org/10.1016/s0263-8231(01)00034-9.
[7] L. Yin, G. Tang, M. Zhang, B. Wang, B. Feng, Monotonic and cyclic response of speed-lock connections with bolts in storage racks, Eng. Struct. 116 (2016) 40–55, https://doi.org/10.1016/j.engstruct.2016.02.032.
[8] L. Dai, X. Zhao, K.J. Rasmussen, Flexural behaviour of steel storage rack beam-to-upright bolted connections, Thin-Walled Struct. 124 (2017) 202–217, https://doi.org/10.1016/j.tws.2017.12.010.
[9] L. Dai, X. Zhao, K.J. Rasmussen, Cyclic performance of steel storage rack beam-to-upright bolted connections, J. Constr. Steel Res. 148 (2018) 28–48, https://doi.org/10.1016/j.jcsr. 2018.04.012.
[10] F. Gusella, G. Lavacchini, M. Orlando, Monotonic and cyclic tests on beam-column joints of industrial pallet racks, J. Constr. Steel Res. 140 (2018) 92–107, doi: 10.016/j.jcsr.2017.10.021.
[11] X. Zhao, L. Dai, K.J. Rasmussen, Hysteretic behaviour of steel storage rack beam-to-upright boltless connections, J. Constr. Steel Res. 144 (2018) 81–105, https://doi.org/10.1016/j.jcsr.2018.01.006.
[12] N. Baldassino, R. Zandonini, Performance of base-plate connections of steel storage pallet racks, in: *Proceedings of fifth international conference on coupled instabilities in metal structures (CIMS2008)* (Sydney, Australia: Gregory J. Hancock Symposium), 2008, pp. 119–130.
[13] F. Petrone, P.S. Higgins, N.P. Bissonnette, A.M. Kanvinde, The cross aisle seismic performance of storage rack base connections, J. Constr. Steel Res. 122 (2016) 520–531, https://doi.org/10.1016/j.jcsr.2016.04.014.
[14] Đ. Jovanović, D. Žarković, V. Vukobratović, Z. Brujić, Hysteresismodel for beam-to-column connections of steel storage racks, Thin-Walled Struct. 142 (2019) 189–204, https://doi.org/10.1016/j.tws.2019.04.056.
[15] G. Gabbianelli, C. Francesco, R. Nascimbene, Seismic vulnerability assessment of steel storage pallet racks, Ing Sismica 37 (2) (2020).
[16] Z. Huang, Y. Wang, X. Zhao, K.S. Sivakumaran, Determination of the flexural behavior of steel storage rack baseplate upright connections with eccentric anchor bolts, Thin-Walled Struct. 160 (2021), 107375, https://doi.org/10.1016/j.tws.2020.107375.
[17] D.A. Padilla-Llano, C.D. Moen, M.R. Eatherton, Cyclic axial response and energy dissipation of cold-formed steel framing members, Thin-Walled Struct. 78 (2014) 95–107, https://doi.org/10.1016/j.tws.2013.12.011.
[18] D.A. Padilla-Llano, M.R. Eatherton, C.D. Moen, Cyclic flexural response and energy dissipation of cold-formed steel framing members, Thin-Walled Struct. 98 (2016) 518–532, https://doi.org/10.1016/j.tws.2015.10.021.
[19] L. Yin, G. Tang, Z. Li, M. Zhang, B. Feng, Responses of cold formed steel storage racks with spine bracings using speed-lock connections with bolts I: static elastic-plastic pushover analysis, Thin-Walled Struct. 125 (2018) 51–62, https://doi.org/10.1016/j.tws.2018.01.005.
[20] L. Yin, G. Tang, Z. Li, M. Zhang, Responses of cold-formed steel storage racks with spine bracings using speed-lock connections with bolts II: nonlinear dynamic response history analysis, Thin-Walled Struct. 125 (2018) 89–99, https://doi.org/10.1016/j.tws.2018.01.002.
[21] E. Jacobsen, R. Tremblay, Shake-table testing and numerical modelling of inelastic seismic response of semi-rigid cold-formed rack moment frames, Thin-Walled Struct. 119 (2017) 190–210, https://doi.org/10.1016/j.tws.2017. 05.024.
[22] J. Proença, I. Rosin, L. Calado, Storage Racks in Seismic Areas, European Commission, Directorate-General for Research and Innovation. Publications Office, Brussels, 2009. https://data.europa.eu/doi/10.2777/60886.
[23] A. Drei, L. Rovere, I. Vayas, D. Jehin, B. Orsatti, A. Kanyilmaz, et al., Seismic Behaviour of Steel Storage Pallet Racking Systems (SEISRACKS2): Final Report, European Commission, Directorate-General for Research and Innovation. Publications Office, Brussels, 2016 https://data.europa.eu/doi/10.2777/686466.
[24] CEN (European Committee for Standardization), EN 16681 Steel Static Storage Systems – Adjustable Pallet Racking Systems – Principles for Seismic Design. Brussels, 2016.
[25] G. Piredda, A. Zonta, E. Bernardi, M. Donà, F. da Porto, Seismic vulnerability of pallet storage systems, in: World Conference on Seismic Isolation (WCSI) 2022: Seismic Isolation, Energy Dissipation and Active Vibration Control of Structures, 2022, pp. 761–770, https://doi.org/10.1007/978-3-031-21187-4_65.
[26] C.A. Castiglioni, A. Drei, H. Mouzakis, A. Kanyilmaz, Earthquake-induced pallet sliding in industrial racking systems, J. Build. Eng. 19 (2018) 122–133, https://doi.org/10.1016/j.jobe.2018.05.004.
[27] C. Brown, J. Stevenson, S. Giovinazzi, E. Seville, J. Vargo, Factors influencing impacts on and recovery trends of organisations: evidence from the 2010/ 2011 Canterbury earthquakes, Int. J. Disaster Risk Reduct. 14 (2015) 56–72, https://doi.org/10.1016/j.ijdrr. 2014.11.009.
[28] M. Donà, L. Bizzaro, F. Carturan, F. da Porto, Effects of business recovery strategies on seismic risk and cost-effectiveness of structural retrofitting for business enterprises, Earthquake Spectra 35 (4) (2019) 1795–1819, https://doi.org/10.1193/041918eqs098m.
[29] A. Filiatrault, P.S. Higgins, A. Wanitkorkul, J.A. Courtwright, R. Michaele, Experimental seismic response of base isolated pallet-type steel storage racks, Earthquake Spectra 24 (3) (2008) 617–639, https://doi.org/10.1193/1.2942375.
[30] A. Franco, S. Massimiani, G. Royer-Carfagni, Passive control of steel storage racks for parmigiano reggiano cheese under seismic accelerations, J. Earthq. Eng. 19 (2015) 1222–1259, https://doi.org/10.1080/13632469.2015.1049386.
[31] M.S.A. Shaheen, K.J.R. Rasmussen, Development of friction damped seismic fuses for steel storage racks, J. Constr. Steel Res. 192 (2022), 107216, https://doi.org/10.1016/j.jcsr.2022.107216.
[32] M. Simoncelli, B. Tagliafierro, R. Montuori, Recent development on the seismic devices for steel storage structures, Thin-Walled Struct. 155 (2020), 106827, https://doi.org/10.1016/j.tws.2020.106827.
[33] M. Ferrari, Lokibase: the device for seismic isolation of pallet racking systems lokibase: Dispositivo per l'isolamento sismico di scaffalature metalliche portapallet, Costr. Met. 3 (2019) 82–91.
[34] M. Ferrari, Lokibase: the device for seismic isolation of pallet racking systems lokibase: Dispositivo per l'isolamento sismico di scaffalaturemetalliche portapallet, Costr. Met. 4 (2019) 111–122.
[35] M. Donà, E. Bernardi, A. Zonta, M. Ceresara, F. da Porto, Effectiveness of load-level isolation system for pallet racking systems, Front. Built. Environ. 8 (2022), 944026, https://doi.org/10.3389/fbuil.2022.944026.
[36] F. Sadek, B. Mohraz, A.W. Taylor, R.M. Chung, A method of estimating the parameters of tuned mass dampers for seismic applications, Earthq. Eng. Struct. Dyn. 26 (6) (1997) 617–635.
[37] A. Reggio, M. De Angelis, Optimal energy-based seismic design of non-conventional tuned mass damper (TMD) implemented via inter-story isolation, Earthq. Eng. Struct. Dyn. (2015), https://doi.org/10.1002/eqe.2548.
[38] C. Moutinho, An alternative methodology for designing tuned mass dampers to reduce seismic vibrations in building structures, Earthq. Eng. Struct. Dyn. (2012), https://doi.org/10.1002/eqe.2174.
[39] D. Pietrosanti, M. De Angelis, M. Basili, Optimal design and performance evaluation of systems with tuned mass damper inerter (TMDI), Earthq. Eng. Struct. Dyn. (2017), https://doi.org/10.1002/eqe.2861.
[40] E. Bernardi, M. Donà, P. Tan, Multi-objective optimization of the inter-story isolation system used as a structural TMD, Bull. Earthq. Eng. (2023), https://doi.org/10.1007/s10518-022-01592-9.
[41] J.M. Kelly, Analysis of fiber-reinforced elastomeric isolators, J. Seismol. Earthq. Eng. 2 (1) (1999) 19–34.
[42] E. Bernardi, M. Donà, A. Zonta, M. Ceresara, S. Mozzon, F. da Porto, P. Tan, Load-level isolation system for industrial racks: Evaluations on a case study structure, in: Proc. of the Eighth International Conference on Structural Engineering, Mechanics and Computation (SEMC 2022), Cape-Town, South Africa, 2022.
[43] M. Donà, A.H. Muhr, G. Tecchio, F. da Porto, Experimental characterization, design and modelling of the RBRL seismic-isolation system for lightweight structures, Earthq. Eng. Struct. Dyn. 46 (2017) 831–853, https://doi.org/10.1002/eqe.2833.
[44] Midas Gen, On-line manual, MIDAS Information Technology Co, Ltd, Korea, 2021. http://manual.midasuser.com/EN_Common/Gen/905/index.htm.2.1.
[45] C. Bernuzzi, A. Gobetti, G. Gabbianelli, M. Simoncelli, Warping influence on the resistance of uprights in steel storage pallet racks, J. Constr. Steel Res. 101 (2014) 224–241, https://doi.org/10.1016/j.jcsr.2014.05.014.
[46] I. Iervolino, C. Galasso, E. Cosenza, Rexel: computer aided record selection for code-based seismic structural analysis, Bull. Earthq. Eng. 8 (2009) 339–362, https://doi.org/10.1007/s10518-009-9146-1.
[47] CEN (European Committee for Standardization), Design of structures for earthquake resistance, part 1: General rules, seismic actions and rules for buildings, in: Eurocode 8, EN 1998–1, CEN, Brussels, 2004.